REPORT DOCUMENTATION PAGE

Form Approved
OMB No. 0704-0188

Public reporting burden for this collection of information is estimated to average 1 hour per response, including the time for reviewing instructions, searching existing data sources, gathering and maintaining the data needed, and completing and reviewing this collection of information. Send comments regarding this burden estimate or any other aspect of this collection of information, including suggestions for reducing this burden to Department of Defense, Washington Headquarters Services, Directorate for Information Operations and Reports (0704-0188), 1215 Jefferson Davis Highway, Suite 1204, Arlington, VA 22202-4302. Respondents should be aware that notwithstanding any other provision of law, no person shall be subject to any penalty for failing to comply with a collection of information if it does not display a currently valid OMB control number. **PLEASE DO NOT RETURN YOUR FORM TO THE ABOVE ADDRESS.**

1. REPORT DATE *(DD-MM-YYYY)*	**2. REPORT TYPE**	**3. DATES COVERED** *(From - To)*
16-10-2009 (rev.)	Final Technical	01-06-2004 to 30-05-2009

4. TITLE AND SUBTITLE

(U) (MURI04) Design, Performance, and Operation of Efficient Ramjet/Scramjet Combined Cycle Hypersonic Propulsion.

5a. CONTRACT NUMBER

5b. GRANT NUMBER
FA9550-04-1-0389

5c. PROGRAM ELEMENT NUMBER
61103F

6. AUTHOR(S)

Paul E. Dimotakis, Graham V. Candler, Lance Jacobsen, Michael Holden, Daniel I. Meiron, and Joseph A. Schetz

5d. PROJECT NUMBER
5094

5e. TASK NUMBER
RS

5f. WORK UNIT NUMBER

7. PERFORMING ORGANIZATION NAME(S) AND ADDRESS(ES)

Graduate Aeronautical Laboratories
California Institute of Technology
1200 East California Boulevard
Pasadena, CA 91125

8. PERFORMING ORGANIZATION REPORT NUMBER

9. SPONSORING / MONITORING AGENCY NAME(S) AND ADDRESS(ES)

Air Force Office of Scientific Research
875 North Randolph Street, Suite 325, Room 3112
Arlington VA 22203-1768

10. SPONSOR/MONITOR'S ACRONYM(S)

11. SPONSOR/MONITOR'S REPORT NUMBER(S)

12. DISTRIBUTION / AVAILABILITY STATEMENT

Approved for public release. Distribution is unlimited.

13. SUPPLEMENTARY NOTES

14. ABSTRACT

This report documents a collaborative research effort among Caltech, the CALSPAN Research Center at SUNY at Buffalo, the University of Minnesota, and Virginia Tech., spanning from June 2004 to May 2009, under AFOSR sponsorship, with program management by Dr. J. Tishkoff. The work focused on fundamental issues related to and derived from the design, performance, and operation of efficient ramjet/scramjet combined-cycle hypersonic propulsion. The work combined experiments in a variety of facilities; numerical simulations employing large-eddy simulations with subgrid-scale (LES-SGS) modeling, detached eddy simulations (DES), and, where appropriate, Reynolds-averaged Navier-Stokes (RANS) simulations; modeling; and diagnostics-/instrumentation-development efforts. Significant accomplishments include quantitative measurements of molecular mixing in scramjet-like flows ranging from high subsonic to supersonic Mach numbers, grid-converged validated LES-SGS of such flows, the development of highly efficient hybrid RANS-DES-LES simulations of non-reacting and reacting scramjet-combustor flows that correctly capture flow behavior; unique experimental data on scramjet combustors and propulsion-mode switching in fully simulated hypersonic flows; and the development of new diagnostics such as arrayed micro-probe, heat-flux, and skin-friction sensors.

15. SUBJECT TERMS
Turbulence, mixing, combustion, high-speed propulsion, propulsion-mode switching, large-eddy simulations, subgrid-scale modeling.

16. SECURITY CLASSIFICATION OF:			**17. LIMITATION OF ABSTRACT**	**18. NUMBER OF PAGES**	**19a. NAME OF RESPONSIBLE PERSON**
a. REPORT	**b. ABSTRACT**	**c. THIS PAGE**			Julian Tishkoff
Unclassified	Unclassified	Unclassified	UL	55	**19b. TELEPHONE NUMBER** *(include area code)* 703-696-8478

GRADUATE AERONAUTICAL LABORATORIES
CALIFORNIA INSTITUTE OF TECHNOLOGY
Pasadena, California 91125

DESIGN, PERFORMANCE, AND OPERATION OF EFFICIENT RAMJET/SCRAMJET COMBINED-CYCLE HYPERSONIC PROPULSION

Paul E. Dimotakis (PI), Caltech
Graham V. Candler (Co-PI), U. Minnesota
Lance Jacobsen (Co-PI), Virginia Tech
Michael S. Holden (Co-PI), State U. of New York at Buffalo
Daniel I. Meiron (Co-PI), Caltech
Joseph A. Schetz (Co-PI), Virginia Tech

Air Force Office of Scientific Research
AFOSR Grant FA9550-04-1-0389

Final Performance Report
1 June 2004 – 31 May 2009

Original: 27 August 2009
Revised: 15 October 2009

California Institute of Technology
State University of New York at Buffalo
University of Minnesota
Virginia Polytechnic Institute and State University

Summary/Overview

This is the final report on a collaborative research effort among four institutions: the California Institute of Technology (Caltech), Virginia Polytechnic Institute and State University (Virginia Tech.), the University of Minnesota, and the CALSPAN Research Center at the State University of New York at Buffalo (CUBRC). The research is aimed at fundamental issues related to and derived from design, performance, and operation of efficient ramjet/scramjet combined cycle hypersonic propulsion. The work combines experiments, numerical simulations, modeling, and a diagnostics-/instrumentation-development effort. The work undertaken spanned the period from June 2004 to May 2009.

Technical discussion

The research was partitioned among the four centers, with experimental and diagnostics work conducted at Caltech, CALSPAN, and Virginia Tech, and various types of simulation work conducted at all four, with a target and research themes as described below per center. All work and results were shared and leveraged in support of the overall effort.

Caltech

Research at Caltech focused on experimental investigations of fundamental aspects of mixing and combustion in turbulent, subsonic, and supersonic flows and simulation of three-dimensional compressible flows relevant to injection problems in air-breathing propulsion applications.

Initial experimental work on compressible turbulent mixing under this grant was centered on studying the flow control and mixing achieved in a low total-pressure-loss, expansion ramp geometry (Fig. 1).

Fig. 1. The supersonic shear-layer facility expansion-ramp flow geometry

In this geometry, a high-speed upper (nominally) “air” stream is expanded over a ramp inclined at 30 degrees to the flow. A low-speed “fuel” stream is injected through perforations in the ramp and generates a mixing layer between the two streams. A key feature of this flow is a purposely designed recirculation zone that transports hot products back toward the fuel-injection location and provides a low-strain-rate flameholding region (Johnson 2005, Bergthorson *et al*. 2007).

Figure 2 shows a composite schlieren image from a pair of experiments with a $M_1 = 1.5$ upper stream flow and a lower stream injection resulting in ramp velocity of $U_R = 5$ m/s. The flow expands down the ramp, creating a corrugated mixing layer that interacts with waves reflected off the upper guidewall. The top-wall boundary layer separates upstream of the measurement rake. As found for a subsonic upper stream, this flow can be controlled by varying the mass

injected through the perforated ramp. Figure 3 is a composite schlieren image for a lower stream injection of U_R = 45 m/s and the same top stream conditions, and illustrates the considerable control that can be exercised by such means.

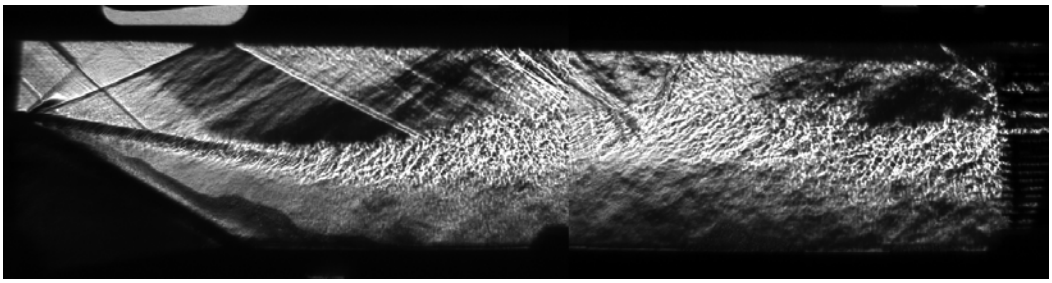

Fig. 2. Composite Schlieren image of the expansion-ramp flow for M_1=1.5 and U_R=5 m/s.

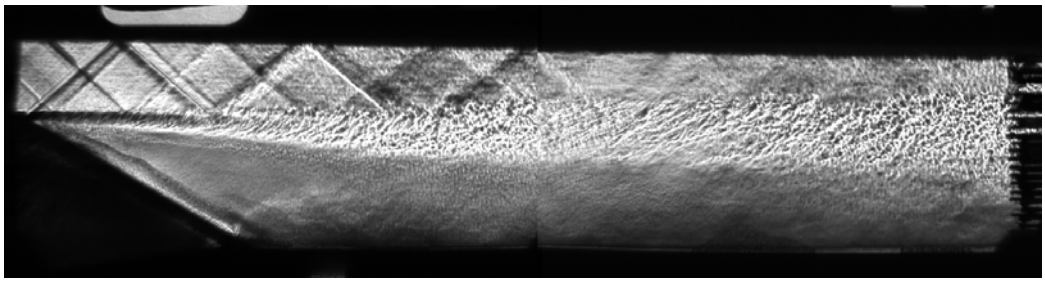

Fig. 3. Composite schlieren image of the expansion-ramp flow for M_1 = 1.5 and U_R = 45 m/s.

The shear layer is almost horizontal, the upper-stream wave system remains uniform, and no boundary-layer separation occurs. A measure of the aerodynamic performance of the device is the overall pressure coefficient, $Cp = (p_e - p_i) / q$, where p_e and p_i are the exit and inlet pressures, respectively, and $q = ½ \rho u^2$ is the dynamic pressure.

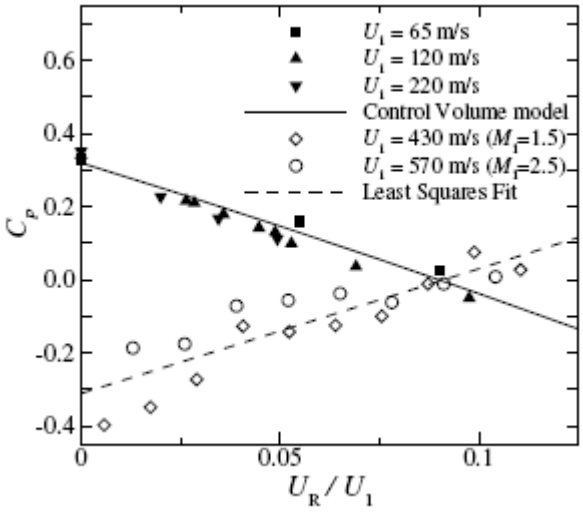

Fig. 4. Measured overall pressure coefficient vs. mass-injection ratio and chemical heat release.

Measured pressure coefficients are plotted in Fig. 4 for the M_1 = 1.5 (diamonds) and 2.5 (circles) for supersonic flow experiments conducted with variable injection and heat release. The slope of this profile has the opposite sign as for subsonic flow (Johnson 2005, filled symbols). Similar to the subsonic-flow results (Johnson 2005), mass injection exerts significant control authority.

Heat release allows the same pressure coefficient to be achieved with a mass injection almost a factor of four lower than for non-reacting flow (Bergthorson *et al*. 2007, Bonanos *et al*. 2008). Molecular scale mixing was measured using the "flip" experiment technique (Mungal and Dimotakis 1984, and Dimotakis 2005). Mixing measurements in this flow geometry were completed at various speeds, up to a top stream Mach number of $M_1 = 2.5$. For an upper-stream Mach number of $M_1 = 1.5$ and a velocity ratio $U_R/U_1 = 0.1$, an estimated 44% of fluid in the duct was mixed at a molecular scale after 4.3 duct heights, and 58% was mixed after 5.4 duct heights. For $M_2 = 2.5$ and $U_R/U_1 = 0.1$, an estimated 47% of fluid was mixed after 5.4 duct heights.

Normalized temperature-rise profiles for the two flip experiments and the estimated probability profile for mixed fluid for $M_1 = 2.5$ flow are shown in Fig. 5 (Bonanos *et al*. 2008). The previously observed trends of decreasing levels of molecular mixing with increasing flow speed (upper-stream velocity) persist.

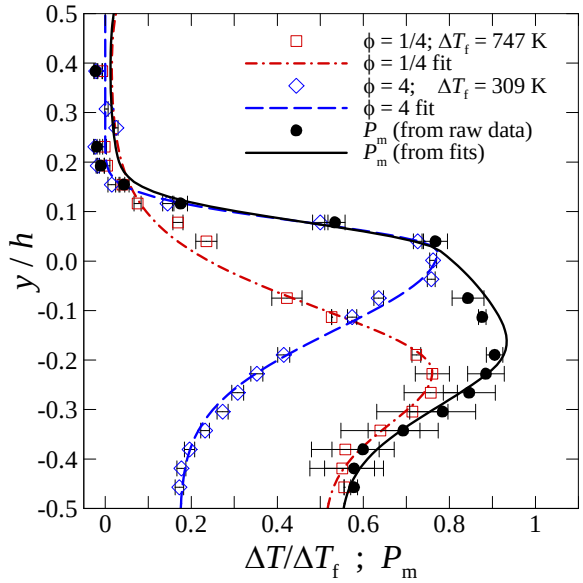

Fig. 5. Normalized temperature and mixed-fluid probability profiles for flip experiments at $M_1 = 2.5$ and $U_R = 60$ m/s.

To explore anticipated further increases in mixing in this flow geometry, the experimental facility was modified to include transverse jets to improve fuel penetration and excite hydrodynamic instabilities in the shear layer. A new splitter plate assembly was designed to incorporate the jets.

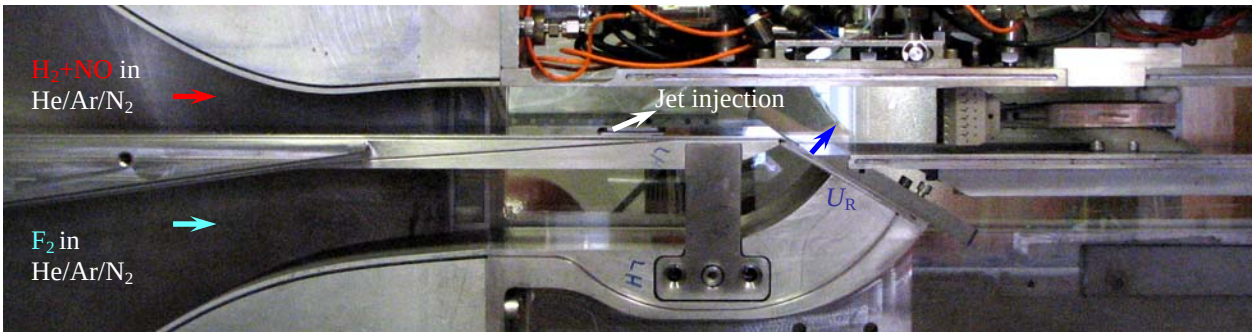

Fig. 6. The new Supersonic Shear Layer Facility incorporates a modular injector block. Mass injection and momentum flux through the angled jets can be varied to control total shear-layer entrainment prior to reattachment, providing active-control means of the mixing zone.

The new test section also allows for variable boundary layer thickness through surface suction or injection and variable height of the expansion ramp (Fig. 6). The modular design of the new facility permits the exploration of several injector geometries and jet orientations. The modified wind tunnel allows supersonic flows with H_2-NO-F_2 chemistry capabilities and can accommodate other fuels and oxidizers.

The chemical kinetics of this system, coupled with the high heat release achievable with moderate reactant concentrations, are important elements.

Preliminary experiments have been conducted at moderate compressibility ($M_1 = 1.5$) in a non-reacting environment and illustrate some of the new phenomenology associated with the interaction between the transverse-jet injection and the shear layer. Color schlieren images from these experiments with a $M_1 = 1.5$ top-stream flow and a ramp-injection velocity of $U_R = 100$ m/s are shown in Fig. 7. The top image is of flow with no jets. The one below is of flow with 5 round jets inclined at 30° with respect to the free-stream and a $\bar{q} = 2.5$. These images indicate the inclined-jet influence on the shear layer.

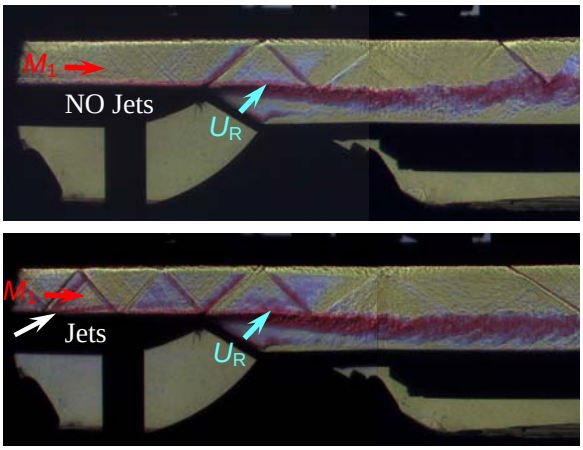

Fig. 7. Color schlieren images of the transverse-jet injection and shear-layer interaction. Experiments have been conducted at various ramp heights.

During the period of performance, the first successful supersonic shear-layer run with reactive jets was performed ($M_1 = 1.5$, 1.95% [H2], 0.1% [NO], 2% [F2], bottom-to-top stream mass flow ratio of 0.12).

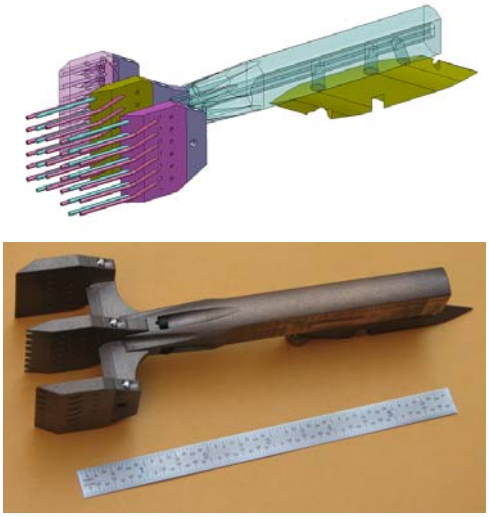

Fig. 8. New modular reconfigurable total-temperature rake.

The flow field generated by the transverse jet injection/shear-layer interaction is highly three-dimensional, and the previous one-dimensional instrumentation rake methodologies relied upon did not permit this flow field to be interrogated. A modular reconfigurable probe rake with 40 channels organized as an 8×5 array of total-temperature probes was designed and fabricated (Fig. 8). Wind-tunnel tests to assess its characteristics and reproducibility were then performed. In order to measure total pressure and Mach number simultaneously, a micro-probe technology was developed based on flow similarities between pointed and blunt cones in axisymmetric supersonic and hypersonic flows (Maddalena *et al*. 2009).

A computational effort was undertaken focusing on flow-field simulations, including turbulent mixing, in the expansion-ramp injection geometry and jets into a supersonic cross-stream. The simulations rely on large-eddy simulation with subgrid scale modeling techniques (LES–SGS) to represent the physics of unresolved scales. The computational framework developed as part of the Caltech Advanced Simulation and Computing (ASC) Department of Energy program (Pantano *et al*. 2007) was used for all simulations. The computational framework has adaptive mesh refinement (AMR) capability, employs advanced low-dissipation finite-difference discretizations with shock-capturing capabilities in supersonic flows, in combination with the stretched-vortex LES–SGS model of Pullin *et al*., and uses the ghost-fluid method for the application of boundary conditions in complex geometries. Prior to the simulation of turbulent flows, the numerical solver was subjected to thorough verification tests (Matheou 2008, and Matheou *et al*. 2008, 2010).

Simulations corresponding to experiments in the expansion-ramp injection geometry with a subsonic top stream show that the structure of the flow and mixing predictions of the LES are in good agreement with experimental measurements, as also discussed in the context of the data depicted in Fig. 10, below. See Fig. 9 that shows the re-circulation flow between the ramp and the reattachment of the shear layer shown in Fig. 3 (bottom) and captured by the LES. The magnitude of the velocity of upstream-moving flow near the lower wall is 10–15% of the top free stream velocity for mass-injection ratios of about 1/10, but becomes negligible as the flow tends towards a free shear layer, for higher mass-injection ratios of about 1/5. The agreement in the pressure coefficient profiles along the top and bottom walls and the total pressure profiles along the transverse direction is satisfactory.

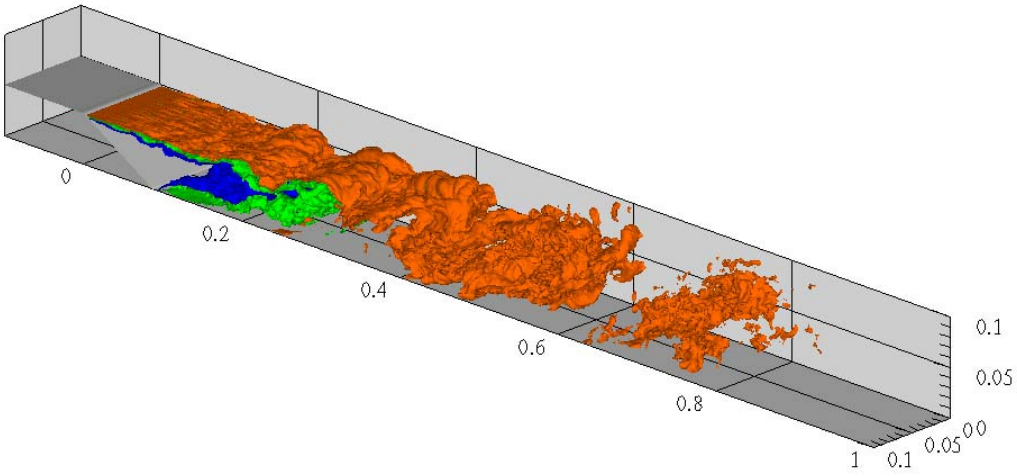

Fig. 9. Instantaneous iso-surfaces of mixture fraction, Z, in the LES of turbulent mixing in the expansion-ramp configuration with a subsonic top stream (M = 0.3). Three iso-surfaces are plotted for Z = 0.2, 0.5, and 0.8. The top stream carries a value of Z = 1 and the bottom Z = 0.

Total (resolved-scale plus subgrid contribution) probability density functions (pdf's) of the mixture fraction were estimated using a presumed beta-distribution model for the subgrid field. The shapes of the pdf's illustrate the improved mixing characteristics of the expansion-ramp geometry compared to free shear layers at equivalent conditions. Mixing statistics were in good agreement with the experimental measurements, indicating that the mixing on a molecular scale is predicted correctly by the LES–SGS model; moreover, statistics were shown to be resolution-independent by computing the flow for three resolutions at twice and four times the resolution of the coarsest simulation. Figure 10 shows a comparison of the mixing statistics between

experiments and simulations. LES results converge for the two highest grid-resolutions used and match the experimental measurements.

In order to access the statistical convergence of the LES average fields and pdf's, a method that compares averages and pdf's over non-overlapping time intervals of the simulation was developed (Matheou *et al*. 2009). The time scale of the statistical variability was found to be significantly shorter than the total time length of the LES. As a consequence, differences observed between the cases simulated cannot be attributed to insufficient statistical convergence. This work was part of the graduate and postdoctoral research of Georgios Matheou and was conducted in collaboration with Carlos Pantano who was at Caltech at the beginning of the period of performance and had moved to University of Illinois at Urbana-Champaign by its end.

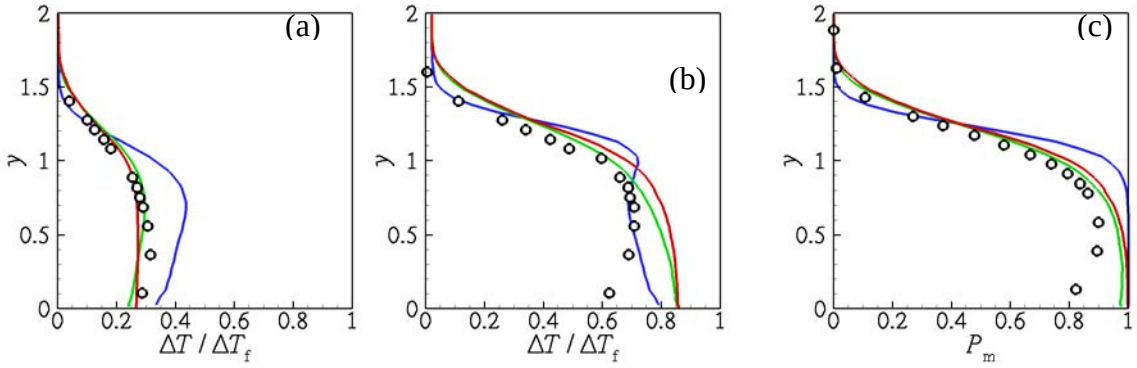

Fig. 10. Normalized temperature rise for H_2-rich (a) and F_2-rich (b) conditions and probability of mixed fluid (c). Symbols correspond to experimental measurements and lines to LES with three grid-resolutions: fine (red), medium (green) and low resolution (blue). Profiles are plotted along the transverse direction, *y*, at the location of the measurement rake about 6 half-duct heights downstream of the ramp-injection.

LES-SGS of an inclined circular helium jet at *M*j = 1 into a supersonic turbulent boundary layer (air at *M* = 3.6) also was performed. In this numerical investigation the jet geometry and flow parameters match those in the experiments of Maddalena *et al*. (2006) with a single injector. The numerical study of Ferrante *et al.* (2009) showed that the main flow features generated by the gas-dynamic interactions of an inclined jet with a supersonic cross-flow, such as barrel shock, Mach disk, shear layer, and counter-rotating vortex pair, are captured numerically by the LES–SGS modeling framework; however, the transition and spatial development of the helium jet were shown to be strongly dependent on cross-flow inflow conditions. These results highlight the importance of correct turbulent inflow conditions for reliable prediction of the dispersion and mixing of a gaseous jet in a supersonic, turbulent cross-flow, as required by the need to simulate fuel injection under these conditions.

A novel methodology for the generation of synthetic turbulent inflow conditions for LES of spatially developing, supersonic, turbulent wall-bounded flows was developed, based on the approach of Ferrante & Elghobashi (2003).[1] This approach was applied to the study of a supersonic turbulent flow over a flat wall interacting with an inclined jet (Ferrante *et al*. 2010), as illustrated in Fig. 11. This work was part of the post-doctoral research of Antonino Ferrante and also was conducted in collaboration with Carlos Pantano, who is presently at the University of Illinois at Urbana-Champaign.

[1] Similar approaches were explored and developed as part of the work undertaken at the University of Minnesota, as described below.

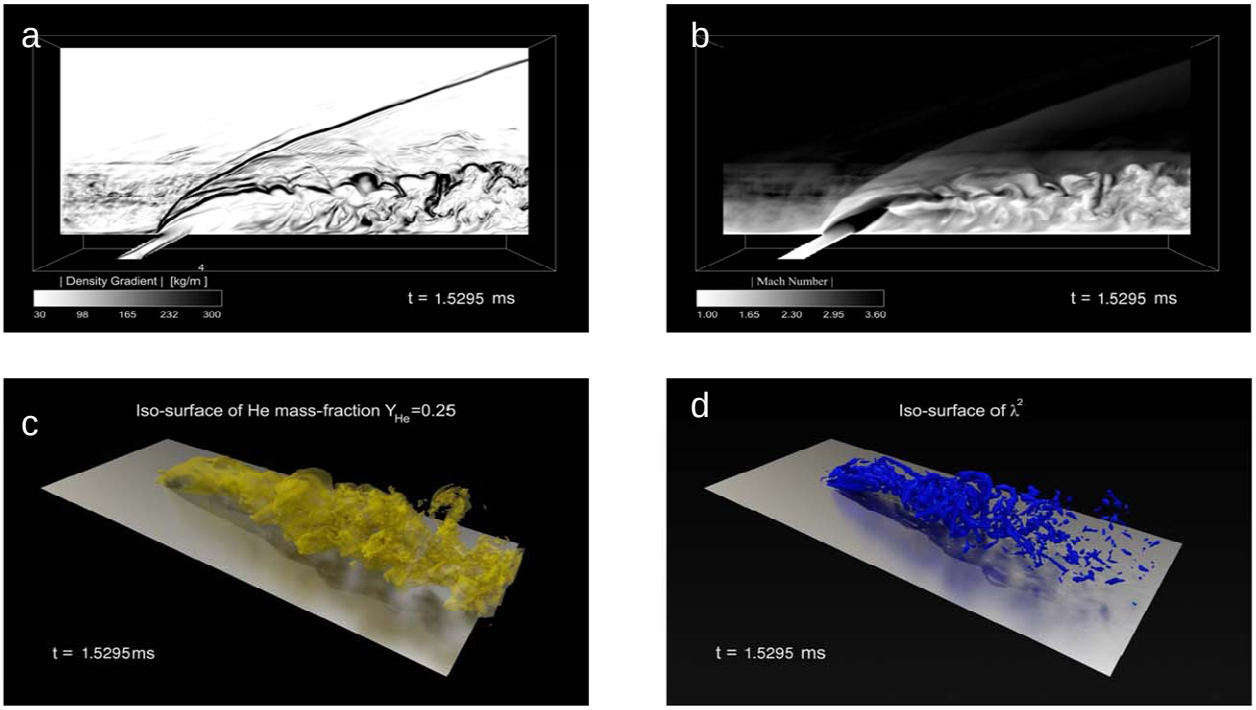

Fig. 11. (a) Instantaneous density-gradient magnitude in the mid-span plane; (b) instantaneous Mach number in the mid-span plane; (c) instantaneous isosurface of helium mass-fraction, $Y_{He} = 0.25$; (d) instantaneous vortical structures identified with the λ_2 method (Jeong & Hussain 1995). Images generated by Paul Adams et al. at the Data Analysis and Assessment Center, U.S. Army Engineer Research and Development Center (HPCMP/DoD), MS 39180, USA. Ferrante *et al*. (2010).

University of Minnesota

Work performed at the University of Minnesota had five major components: the simulation and optimization of inward-turning inlets for scramjets using conventional Reynolds-averaged Navier-Stokes (RANS); the development of a novel approach for transitioning between RANS and large-eddy simulations (LES); the development of a low-dissipation numerical method for finite-volume simulations; simulations of injection into supersonic streams with extensive comparison to experiments; and the simulation of reacting, turbulent flows with a hybrid RANS/LES methodology. All of this work has been documented in conference papers and is in the process of being distilled into archival publications. In this report, we present the key findings of the work and provide the highlights of the five-year MURI program. The reader is referred to the accompanying publications for additional details.

Inward-Turning Flow Simulation and Design Optimization

An efficient inlet is critical to the operation of scramjet-powered hypersonic air-breathing vehicles. The inlet must compress the flow with minimal skin friction, heat transfer, and shock losses, while providing uniform flow to the combustor. Historically, many types of hypersonic inlets have been evaluated, with two-dimensional ramp-like inlets becoming favored. Recently, there has been renewed interest in inward-turning inlets because of their potential for high efficiency, smaller wetted area, and airframe integration considerations.

Previous work has shown that axisymmetric Busemann and streamtraced Busemann inlets are good candidates for hypersonic air-breathing vehicles (Molder and Szpiro 1966, Van Wie and Molder 1992, Kothari *et al*. 1996, and Billig *et al*. 1999, 2000, 2003). Theoretically, these inlets have significantly higher efficiencies than conventional two-dimensional designs; however, real-world performance of these inlets may be affected by finite leading edge truncation angles and bluntness and boundary layer displacement. In Drayna *et al*. (2006), a systematic study of the influence of these design choices on the efficiency of inward-turning inlets for Mach 10 operation was undertaken. It was found that, for the conditions studied, the inlet truncation angle should be kept between 2° and 4°. This range balances increased skin friction and heat-transfer losses with shock losses. Presumably, vehicle system optimization would favor the higher end of this range to reduce cooling requirements. It was found that the leading edge radius should be kept as small as possible, but small radii ($r \sim 1$ mm) give better performance than ideal sharp leading edge inlets because of improved coalescence of compression waves. Finally, an improved boundary layer correction approach was developed, in which the ideal inviscid inlet shape is simulated first, including viscous effects, the resulting displacement thickness is computed, and the inlet shape is modified based on this displacement. It was found that inlet performance is optimized when a fraction of the computed displacement thickness is used. For the present conditions, a 50% correction was found to be best. These guidelines were used in the design of the HyCAUSE and ASET inward-turning inlets under the DARPA FALCON program (Candler *et al*. 2006, 2008).

Additional studies were performed on three-dimensional streamtraced Busemann inlets. It was found that both inlet cross-section and leading-edge shape have a major influence on inlet efficiency and performance. Inlet and leading edge geometries that minimize flow non-uniformity and secondary flow in the boundary layer tend to have improved efficiency. Further work must be done in this area to understand the effects of inlet-profile and leading-edge shape on inlet performance better.

It is very difficult to optimize an inlet through sequential *ad hoc* geometry changes, and it would be infeasible to perform trade studies without a formal optimization process. To address these issues, a CFD-based approach for inward-turning inlet optimization was developed. The main step focuses on the automated generation of high-quality grids based on a parametric definition of the inlet surface. For example, a typical inward-turning inlet geometry can be defined with four cubic rational Bezier curves constrained by the leading-edge lip shape, the shoulder curve (that cancels the shock wave and turns the flow to the axial direction), and the combustor cross-sectional shape. This geometric parameterization allows sufficient design flexibility, on the one hand, while decreasing the control degrees of freedom, on the other. This is illustrated schematically in Fig. 12.

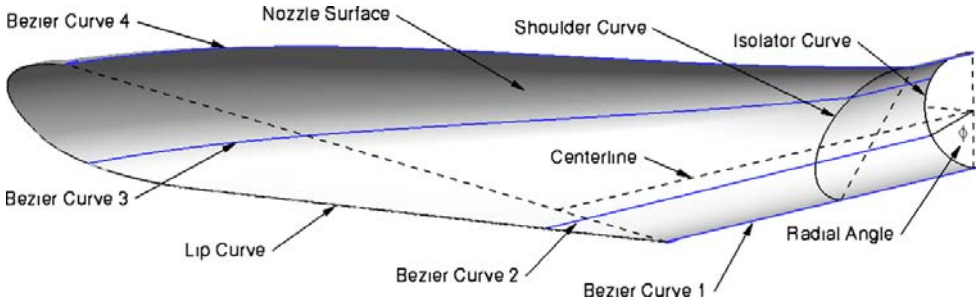

Fig. 12 Parametric surface definition of an inward-turning inlet.

The parametric surface definition serves two purposes: it provides a set of parameters that can drive an optimization process, and it defines the inlet geometry for use in a grid generator. We use the GridPro grid generator because it allows a given grid topology to be reused for new designs. This approach makes it possible to automate the grid generation process for a given set of surface definition parameters completely. It is crucial that the resulting grids are of very high quality for any set of parameters because the optimization process cannot depend on the grid. Figure 13 plots the grid topology (the structure of the individual hexahedral blocks that define the grid) and some slices of a grid. The grid is smoothly varying and is designed to capture the boundary layers, leading edges, and other key features. Typical grids are composed of 5-10 $\times$ 10^6 hexahedral elements. An example of a CFD solution is shown in Fig. 14.

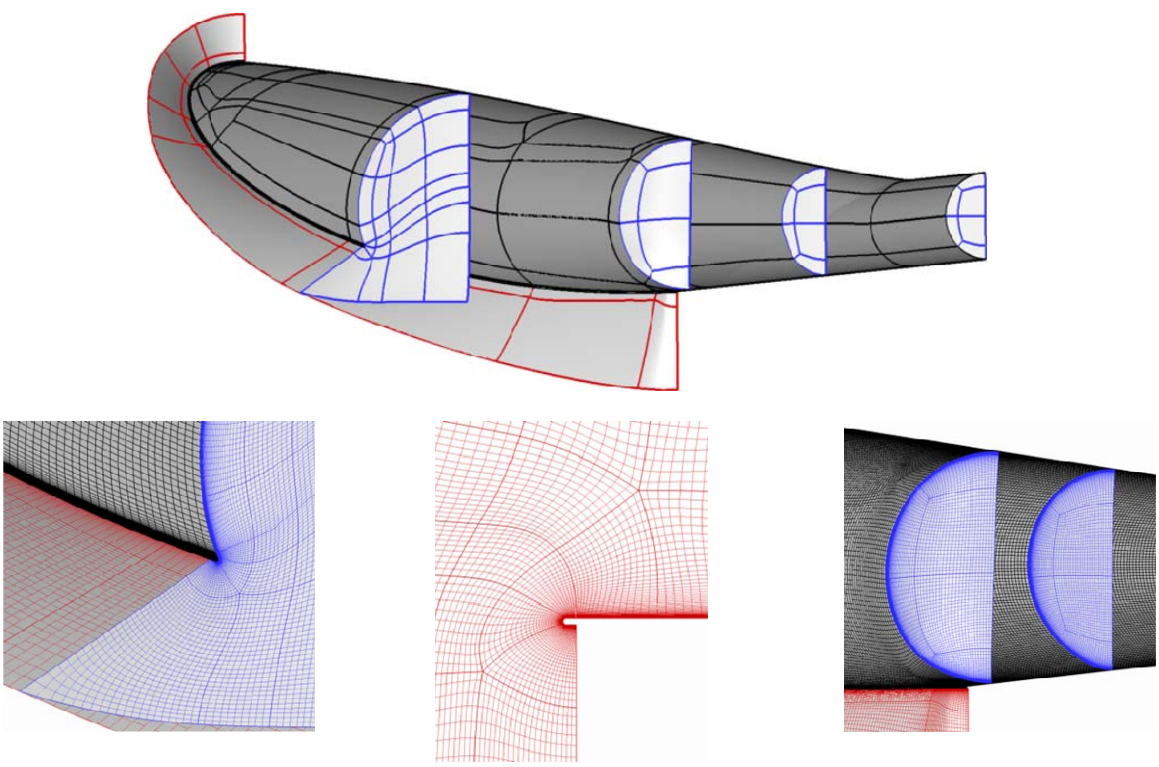

Fig. 13 Grid topology and representative grid surfaces for an inward-turning inlet.

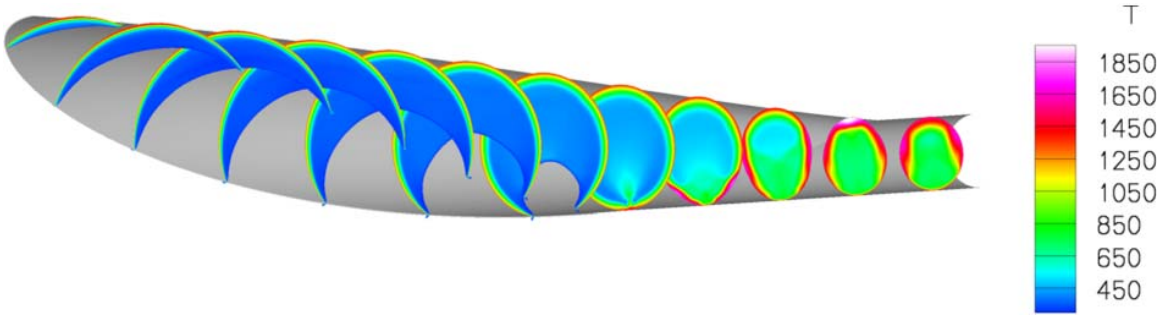

Fig. 14 Computed temperature distribution within an inward-turning inlet.

The steps required to perform a single-point design optimization are:

1. Start with a candidate shape, compute a laminar solution, and estimate the boundary layer trip location using an appropriate criterion. Hold this axial location fixed for all subsequent designs.

2. Perform a design of experiments study to identify a good starting point for a more detailed design.
3. Select the optimal starting point, using minimum drag, for example.
4. Perform a gradient-based optimization by varying the surface definition parameters.

This process requires that each step be orchestrated with a control code that is responsible for selecting geometric parameters, generating the grid, transferring files between computers, running the CFD cases, post-processing the data, and driving the design to an optimum. We use the modeFRONTIER code (Esteco 2009) for this process.

A number of optimization studies were performed using the approach outlined above (Candler *et al.* 2008). They indicate that it is possible to obtain significant improvements in inlet efficiency, although the choice of the best objective function is an open question. For example, choosing to minimize drag may result in an inlet with strong shock waves in the isolator. These shocks impinge on the surface downstream of the combustor exit plane and, as such, do not cause drag; however, they are undesirable.

A RANS-to-LES transition approach

The simulation of the flow within a scramjet engine must resolve a significant range of energy-containing length and time scales. Many of the target flow fields for these computations involve an inflow boundary where space and time-varying velocity fields must to be specified. The velocity specified at these boundaries must reflect the space and time scales the numerical method intends to resolve. If the inflow consists of an incoming boundary layer, the range of structures known to be present (horseshoe vortices, streamwise vortices, etc.) must be represented, ideally with the correct spectrum, root-mean-square (RMS) values and phase information. For example, in computations of mixing layers, computing the developing boundary layers on the splitter plate would use a significant fraction of available computing resources. Instead, boundary-layer profiles computed using cheaper means (such as RANS or experimental profiles) could be specified at the trailing edge of the splitter plate and augmented with perturbations of flow variables. A brief but comprehensive survey of current inflow generation methods can be found in Keating *et al.* (2004).

In this portion of the work under the MURI program, a means of generating realistic turbulent flow fields (specifically for turbulent boundary layers) was developed using the attached-eddy hypothesis (Subbareddy *et al.* 2006). The idea is relatively simple. Consider a domain that extends a small distance (of the order of a few boundary layer thicknesses) upstream of the inflow boundary. A separate, ‘precursor’ calculation is run on this domain using an inexpensive RANS method to establish the mean velocity profiles and thermodynamic profiles for compressible flow at the inflow plane that is set to be the exit plane of the precursor grid). In many cases, these profiles can be verified or supplemented using existing experimental data.

The next step is to distribute a collection of eddies in the plane of the wall and use the Biot-Savart law to compute the associated velocity field. A variety of distributions could be used. Depending on the level of sophistication required, one could use a random distribution or arrange them in trains to correspond with the notion of ‘packets’. The restriction is that the fluctuating velocity field should reproduce the correct first- and second-order statistics (mean profiles, RMS values, spectra, and Reynolds stresses) to certain fidelity. The distribution of eddies provides a box of data that can be introduced in a time-dependent manner through the inflow plane. One could choose the box size such that the ends are uncorrelated, which would enable use of the data in a time-periodic manner. Increasing the size of the box does not place undue demands on the

computation, since the precursor 'box' is set up prior to the actual simulation. A step-by-step procedure for constructing such an inflow box of attached eddies is given in Keating *et al.* (2004). An example of an 'eddy box' is shown in Fig. 15.

This synthetic turbulent inflow has been applied to a wide range of flows relevant to scramjet engines. For example, Fig. 16 shows a comparison of experimental data and simulations for the injection into a supersonic crossflow (Barber *et al.* 1997). Here, injectant mass-fraction contours are plotted on a plane located 97 effective jet-diameters downstream of the injection location. Three simulations are shown: a detached eddy simulation (DES) with an unsteady (eddy box) inflow; a DES with a steady inflow; and a conventional RANS. Here, the DES attempts to resolve the large-scale inertia-driven unsteady flow physics, and a model for the turbulent boundary layer near the wall is used (more details are provided below). Without the unsteady synthetic turbulent boundary layer inflow, the DES result can be seen to be excessively coherent, resulting in a small plume of high injectant mass fraction. Additional studies show that using this type of inflow may be critical for obtaining accurate results when unsteady flow field simulation methods are used (the wide class of DES and hybrid RANS/LES approaches).

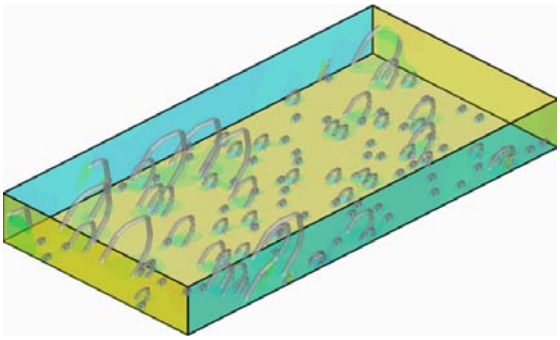

Fig. 15. Hairpin vortices in a sample eddy box visualized in terms of swirl strength of the velocity-gradient tensor.

Numerical Methods

The simulation of the highly unsteady flows found within a scramjet combustor places stringent demands on the numerical method employed. The method must be robust and capable of accurately capturing all regions of the flow, including those with large gradients such as shock waves and contact surfaces. It also must be amenable to non-ideal grids so that complex geometries can be modeled. Conventional upwind-biased methods widely used in the aerospace community are excessively dissipative for many applications, particularly when grid size becomes a limiting factor. As part of the work undertaken, a wide range of methods were explored and assessed. In this section the main findings related to numerical methods are summarized. The reader is referred to the papers resulting from this work and particularly to Subbareddy and Candler (2009).

The University of Minnesota MURI simulations relied on the US3D code (Nompelis *et al.* 2005), which solves the compressible Navier-Stokes equations using a hybrid structured/unstructured cell-centered finite-volume approach. The default approach evaluates inviscid fluxes using the modified Steger-Warming flux vector splitting. Evaluation of fluxes at cell faces using second-order upwind reconstruction was used with great success in simulating steady-state supersonic and hypersonic flows but is too dissipative to allow turbulence to be captured in LES applications. A third-order, upwind-biased flux reconstruction therefore is used here. The third-order upwind-biased reconstruction is still robust but not overly dissipative. Viscous fluxes use

gradients calculated via a weighted least-squares approach. This approach is feasible provided great attention is given to grid resolution studies and large grids are used to limit numerical dissipation. This work indicates that a method specifically designed for low numerical dissipation would greatly reduce costs of these simulations, as independently concluded from the simulation work at Caltech. A candidate method developed at Minnesota with MURI funding is under going evaluation and will be briefly discussed below.

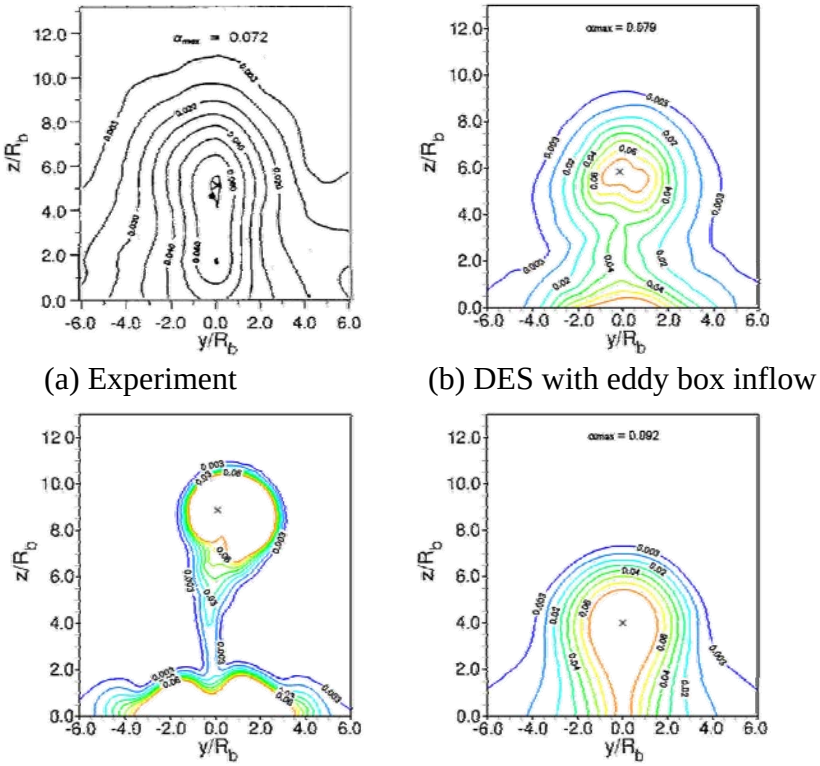

Fig. 16. Helium mass fraction contours for normal injection at x/R_b = 97 from injection port.

Time integration in the solver is backward-Euler and formally first-order-accurate. The time steps used are small enough, however, that using a formally second-order-accurate time-integration scheme did not alter the results significantly. The solver uses the Full-Matrix Point Relaxation (FMPR) method, which is fully implicit. This method removes the impractical time-step limitation of explicit methods, particularly on grids with tight boundary-layer clustering, as used in the present simulations.

The idea of the new low-dissipation approach for the LES of compressible flows is introduced here. The full derivation of the method and its application to several test cases are given in Subbareddy and Candler (2009). Ideally, numerical schemes used in large-eddy simulations of compressible flow have the following properties: they are (i) conservative, (ii) capable of capturing shocks, (iii) non-dissipative in regions of the flow that are smooth, and (iv) stable. Conditions (i) and (ii) are not too problematic. Discretizing the conservative form of the governing equations ensures that mass, momentum and total energy are conserved. Shock-capturing methods of various degrees of sophistication exist in the literature and are relatively well studied.

For condition (iii), low-dissipation schemes have been constructed by selectively switching on the dissipative portion of the numerical flux in regions of the flow where discontinuities are detected (the fluxes used in most shock capturing methods can be written as the sum of a symmetric, non-dissipative part and a dissipative portion). Detecting shocks and discontinuities in a robust and efficient manner is a topic of current research; however, several shock-detecting switches have been proposed and shown to be effective over a range of flow conditions. Assuming that shock-capturing and detection mechanisms perform adequately, one is left with the problem of ensuring that the non-dissipative symmetric fluxes produce stable solutions. Numerical instability is especially problematic in non-dissipative LES of turbulent flows. By construction, these solutions typically have substantial energy at all resolved wavenumbers -- the Nyquist wavelength of the grid is usually close to the LES filter length scale, which is usually in the inertial range of the energy spectrum and has large energy content (both in theory and in the numerical solution for non-dissipative schemes). In these situations, aliasing errors arising from the non-linear convective terms in the Navier-Stokes equations are significant and produce an energy pile-up in aliased wavenumbers, eventually causing solutions to blow up if they are not contained. Aliasing errors typically arise with high-order methods (because low-order methods do not represent the largest wavenumbers accurately). Indeed, the first de-aliasing methods were designed for pseudo-spectral simulations; however, low-order central-difference approximations, or symmetric finite-volume fluxes, are also susceptible to instability and aliasing, and strategies to stabilize the solutions were shown to work well for both high-and low-order schemes.

For compressible flows, two main approaches exist for dealing with stability problems. Firstly, writing the convective terms in the skew-symmetric form results in reduced aliasing error amplitudes, relative to divergence and advective forms. These properties were shown using pseudo-spectral simulations of Burgers' equation and compressible isotropic turbulence. Ducros *et al*. (2000), derived a set of second and fourth-order accurate, conservative skew-symmetric-like fluxes for finite-volume methods with de-aliasing in mind. Skew-symmetric splitting has been used for DNS and LES computations of compressible flows.

The second approach uses the idea of secondary conservation laws -- essentially additional equations in conservation-law form for quantities (such as entropy) derived from the primary conservation equations. Under certain conditions, such secondary quantities are called *entropy functions* and the corresponding fluxes *entropy fluxes*. An entropy function can be used to generate a vector of entropy variables that can be mapped uniquely with the vector of conserved variables. Entropy variables then are used to enhance numerical stability.

In this context, one can consider the equation for kinetic energy. For incompressible flows, the evolution of kinetic energy is represented implicitly by the evolution of the velocity field. An equation for kinetic energy can be derived by multiplying the momentum-component equations by the velocity components and summing. Recently, it was shown that writing the discrete fluxes of the momentum-component equations in a form that makes the implied flux of kinetic energy conservative ensures that the net change of kinetic energy in the computational domain is traceable only to boundary contributions and viscous dissipation. This approach vastly improves the stability of the calculations.

For compressible flows, the equation for kinetic-energy transport is derived from the conservation equations for density and momentum. In the absence of heat release or other energy addition, it is not an independent equation; however, in most formulations, it is combined with the internal energy to yield a set of equations in conservation form, which is important for flows with shocks. Concentrating on the terms representing the flux of kinetic energy and its rate of change, which appear in the total energy equation, one can show that these terms can be obtained

from the corresponding terms in the PDEs for the continuity and momentum equations. For spatial fluxes, ensuring that the discrete equations are consistent as well yields a simple set of constraints, similar to the incompressible-flow formulation, as well as the skew-symmetric form. Ensuring that the discrete time derivatives are consistent yields a novel density-weighted Crank-Nicolson-like scheme.

The new method has been used to simulate injection into a supersonic crossflow. Initial results show that it dramatically decreases dissipation levels in the simulation. For some cases without strong shock waves it is possible to run the simulation without any numerical dissipation. Such a method could revolutionize the simulation of scramjet flows.

Simulations of injection in supersonic crossflow

The approach taken for simulating the injection flowfield is a hybrid RANS/LES methodology. For some simulations, the blending of the RANS and LES portions is handled by the standard DES equations, now referred to as DES97. The one-equation Spalart-Allmaras (SA) model with the density corrections of Catris and Aupoix (2000) is used as the background RANS model for DES. The DES equations are not used in the natural mode, where the boundary layers are very thin compared to the wall-parallel spacing of the grid so that they are fully within the RANS portion of the simulation. Instead, the DES equations are used as a wall-modeled LES (WMLES), where the RANS portion acts as a wall model for the LES portion. To reduce simulation costs, one would also like to use the RANS portion throughout the attached boundary layers, in regions where mixing of fuel and air does not occur. There are, however, some known issues when using DES in this way.

DES97 was investigated first as a wall model for LES by Nikitin *et al*. (2000). In their channel flow simulations they identified the log-layer mismatch in which a velocity jump occurs between the modeled and resolved portions of the log layer at high Reynolds numbers. The the velocity jump results in under-prediction of the skin friction.

Another issue is maintaining RANS behavior in attached boundary layers where the grid is highly resolved. In DES97, RANS and LES regions are determined only by grid spacing. The more refined the grid becomes, the closer to the wall the switch moves. Thus, on grids with wall-parallel spacing much smaller than the boundary layer thickness, DES97 switches to LES mode within the boundary layer. This switch reduces eddy-viscosity levels in the boundary layer below those needed to maintain proper RANS behavior and can lead to the phenomenon referred to as grid-induced separation.

Recently, the delayed detached-eddy simulation (DDES) method was developed to allow for RANS behavior to be maintained inside attached boundary layers, regardless of wall-parallel spacing. This was accomplished by replacing the RANS/LES switch with a new formulation that makes the switch a function of not only the grid but also the local solution. If the eddy viscosity is large and no LES content (resolved velocity fluctuations) is present, the model operates in RANS mode, even if the grid is very fine. DDES, however, still is intended for natural DES applications, primarily for external flow fields. DDES also can be used as a WMLES, but, as it was not developed specifically for WMLES, it does not solve the problem of log-layer mismatch.

Interest in using the DDES concept for WMLES applications led to further improvements to the formulation aimed at resolving the issue of log-layer mismatch. These improvements, when used with the SA model as the background RANS model, are referred to as the Hybrid-SA model. Simulations presented here also will make use of the Hybrid-SA model. No changes to any of the functions or constants contained within the Hybrid-SA model have been made for the current

study; however, the model was calibrated using low-speed, incompressible flow. Thus, the Hybrid-SA model may not be optimized for the high-speed, compressible flow of interest in the context of this work.

Grid generation is of critical importance in simulating scramjet fuel injection. High resolution is necessary in the jet shear layer to capture the turbulent breakdown of the jet plume as it mixes with the freestream gas. Adequate grid resolution is of particular importance near the injector port exit, where the jet begins to break down. This high resolution cannot be carried into other domain regions, however, as the total cell count would make the calculation prohibitively expensive. In addition to the resolution requirements, a high level of isotropy is desirable for the LES regions of the grid, which comprise a large portion of the total-element count. Any changes in the spatial resolution of the grid must occur smoothly.

The grids used in this work are generated using the commercial grid-generation package GridPro (Program Development Corp. 2009). Although the solver is built with an unstructured grid framework, the grids used for the present simulations do not contain tetrahedral or prismatic elements. They are composed entirely of structured-like hexahedral cells because hexahedral grids are found to provide a higher quality solution than a tetrahedral grid with a similar total-element count. Also, the hexahedral elements are more efficient at filling volume. The unstructured grid framework does, however, allow for an arbitrary level of complexity in the all-hexahedral grid. This approach allows for the use of advanced grid-generation techniques that can handle complex geometries and make efficient use of grid elements, which is an enabling factor in these simulations.

The grids contain a core of high-density cells in the jet region and then rapidly, but smoothly, coarsen outside of core region, as seen in Fig. 17. The figure shows a grid with identical topology and relative grid density to grids used for this study; however, the grid in the figure has been coarsened significantly for clarity. The grid along the walls near the injector port is swallowed into the injector nozzle. The cell density is much higher near the injector exit than in the downstream region. While not shown in the figure, the grid is stretched to the walls to resolve large gradients in the boundary layer. The first cell off of the wall is within one wall unit.

The grids extend into the injector plenum chamber. Typically, the total temperature and total pressure in the plenum chamber are known. Using these values with a characteristic-based subsonic boundary condition has been found to work well when the grid extends into the plenum, reproducing the proper mass flow rate values for cases where a value was given. If the plenum is not included and only a straight section of injector nozzle is used, the total pressure must be reduced to achieve the proper mass-flow rate. The latter approach can be problematic if the mass flow rate through the injector is not known, as is the case with the configuration being simulated here.

Simulations were performed using both DES97 and Hybrid-SA turbulence models on two grids with different resolution levels. Each run is started by initializing the flow as a RANS simulation. This initial simulation establishes the mean flow features, such as shocks and the jet plume, and stabilizes the mass-flow rate, which tends to oscillate for some time because of the shape of the plenum chamber and the way the flow is initialized. The simulation then is changed to the DES97 mode and run for many flow-through times (on the order of 50), where a flow time is defined as the jet diameter divided by the freestream velocity, to allow the unsteady flowfield features to develop fully. Only after the flow has been allowed to develop sufficiently are flow statistics accumulated.

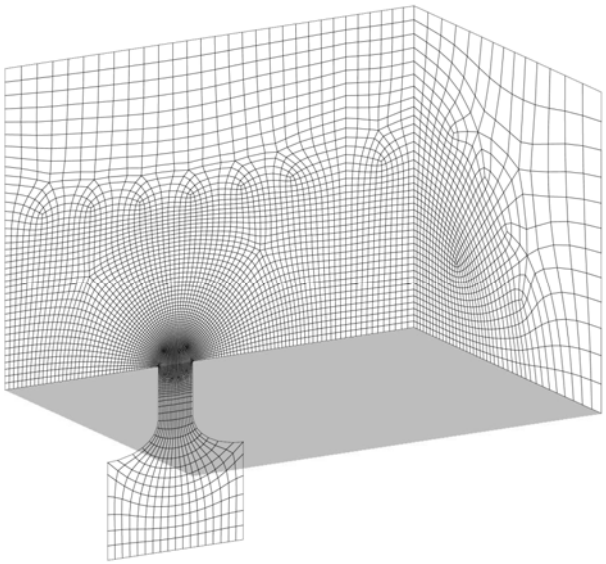

Fig. 17. Slices of the grid used for normal injection into supersonic crossflow. The resolution has been greatly reduced from the levels used in the simulations for display clarity.

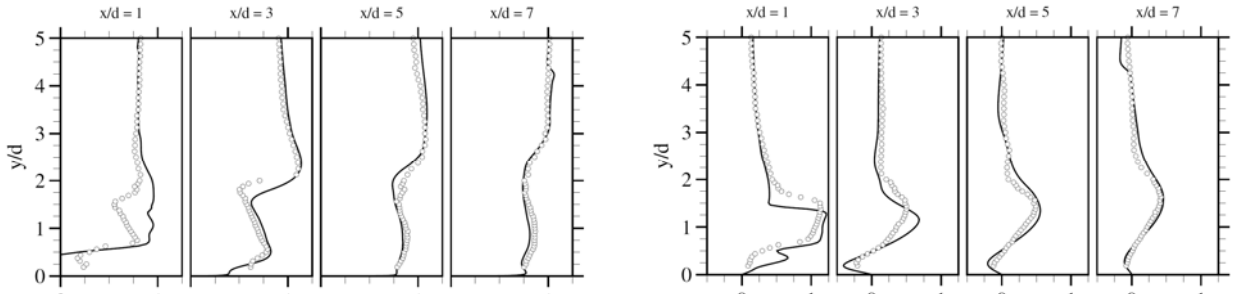

Fig. 18. Normalized mean streamwise and wall-normal velocity profiles at various downstream locations along the tunnel centerline. Symbols: experiment; lines: Hybrid simulation.

Profiles of mean streamwise and wall-normal velocity components at several stations downstream of the injector port are shown in Fig. 18. The profiles are positioned along the tunnel centerline at downstream locations of x/d = 1, 3, 5 and 7. In the figure, the velocities have been normalized by the freestream velocity. The scales of each of the four axes in each plot are identical. The symbols show the Laser Doppler Velocimetry (LDV) measurements from the experiments of Santiago and Dutton (1997), and the solid lines show the results of the Hybrid-SA simulation on the finer grid.

The profile at x/d = 1 passes through the barrel shock of the jet plume. The streamwise velocity is nearly constant above y/d = 3. Below y/d = 3, the experiment shows a slight increase in streamwise velocity before a sharp decrease down to y/d = 1.5. The nearly linear region is within the barrel shock. Below y/d = 0.75, there is again a sharp decrease in streamwise velocity in the experiment as the profile enters the low-speed wake below and behind the barrel shock. Simulation results deviate from the LDV data in the barrel shock region. The simulation predicts a larger and more uniform streamwise velocity within and directly above the barrel shock. Low-speed flow also is found below the barrel shock in the simulation; however, while the velocities in the experiment remain positive, the simulation predicts an area of reverse flow. Agreement within the barrel shock region is better for the wall-normal velocity. Both experiment and

simulation predict a maximum wall-normal velocity that is greater than the freestream velocity. This maximum occurs in the upper part of the barrel shock.

The profile at y/d = 3 is completely downstream of the barrel shock. The streamwise velocity within the wake of the jet plume is slower than the flow outside of the jet. The shear layer between these two regions is clearly visible around y/d = 2. The simulation predicts a slightly thicker shear layer than seen in the experiment. Otherwise, the agreement between the simulation and LDV measurements is very good. The jet plume also is marked by an area of increased wall-normal velocity that is attributable to the presence of the counter-rotating vortex pair (CVP) that forms within the jet plume. As the flow moves downstream, the streamwise velocity within the jet plume approaches that of the surrounding flow, reducing the velocity jump across the shear layer. The shear layer thickens as more fluid is entrained within the jet plume, and it also moves further from the wall. The CVP weakens as the vortices move downstream, resulting in lower peak wall-normal velocity within the jet plume. At x/d = 5 and 7 the magnitudes and locations of the peak in wall-normal velocity predicted by the simulation agree well with the LDV data. More details of these comparisons are available in a paper submitted for publication (Peterson and Candler 2009).

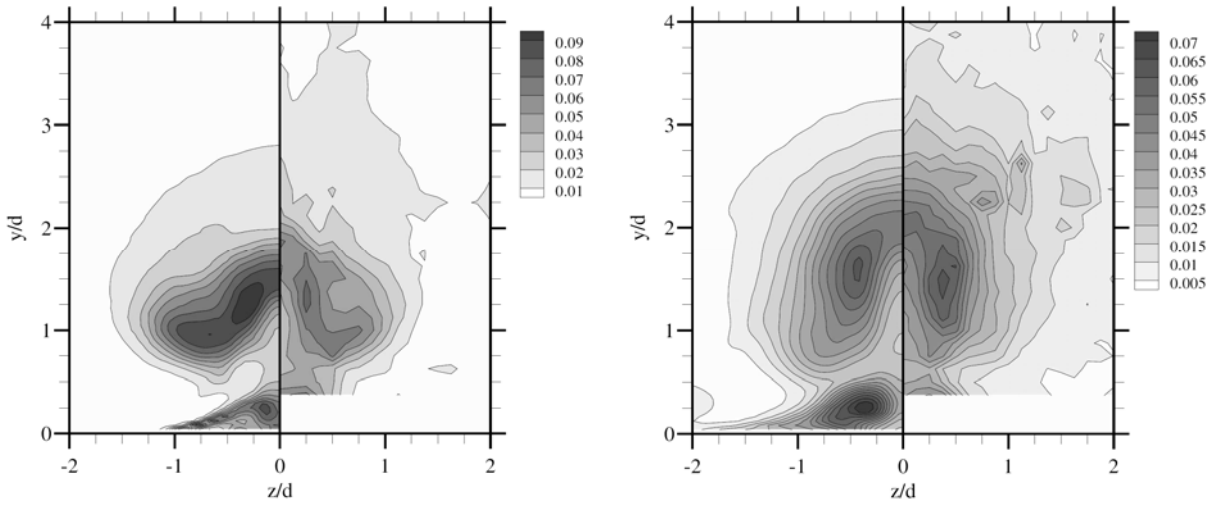

Fig. 19. Normalized TKE contours at planes x/d = 3 and x/d = 5. Left half of each plot shows Hybrid simulation; right half shows LDV data.

Turbulence intensities were also measured with LDV by Santiago and Dutton (1997). Non-dimensional turbulent kinetic energy (TKE) contours are shown for the crossflow planes at x/d = 3 and 5 (Fig. 19). The right half of each plot shows the TKE measured by LDV. The left half of each plot shows the resolved TKE from the Hybrid-SA simulation on the fine grid. As before, the simulation data have been averaged across the plane of symmetry.

Qualitatively, the shape of the TKE contours in the simulation is consistent with that seen in the experimental measurements at both planes. At x/d =3, the trends in TKE contours are similar to what was seen for the mean streamwise velocity. Plume heights are also similar, but the spanwise width of the contours extends farther from the centerline in the simulation than is seen in the experiment. The quantitative values of TKE in the core of the jet plume are generally larger in the simulation than in the experiment. The maximum value of non-dimensional TKE in the simulation is 0.1, whereas the maximum measured value is 0.075. Santiago and Dutton reported significant asymmetries in turbulence quantities at this plane. The simulation results show much less asymmetry.

Quantitative agreement is improved at the $x/d = 5$ plane. Within the jet plume, the resolved TKE is found to take values very consistent with the experiment. The peak value of non-dimensional TKE in the jet plume is found to be approximately 0.61 for both the simulation and LDV data, with the peak value located slightly farther from the wall in the simulation. In this plane, the global maximum in TKE for the simulation occurs in the wake vortices, below the jet plume. The maximum value in this region is 0.75. Only the top portion of the wake vortices was measured in the experimental results.

Plots of the non-dimensional Reynolds stress contours from the simulation are qualitatively very similar to the experiment. In both planes, a region of large negative correlation is found in the region corresponding to the outer boundary of the jet plume, where the large Kelvin-Helmholtz circumferential rollers are found.

Overall, the simulations were successful in resolving the large-scale turbulent features in the jet plume, as well as the unsteady separation region upstream of the injector. Qualitative flow visualizations from the simulations compare well with flow visualizations from experiments. Quantitative comparisons to mean velocity fields were generally good. Comparisons with turbulence measurements were also favorable. The magnitudes and distribution of the turbulent kinetic energy resolved in the simulations are consistent with those measured in the experiment, with better quantitative agreement found at the more downstream measurement location. Agreement is also good for the Reynolds stress.

Simulations were performed on two grids of different resolution. The finer grid had 1.5 times the resolution in each direction of the coarser grid. A larger range of turbulent structure was resolved on the finer grid, but resulting velocity statistics were similar in the jet plume on the two grids. Thus the bulk of the turbulent kinetic energy of the jet plume is in the structures that can be resolved with the coarser grid resolution; however, when using a mean RANS boundary-layer profile as an inflow condition for the Hybrid-SA model, as is done here, the encroachment of the RANS mode into the separation region upstream of the injector can prevent the unsteady structure from developing in the jet plume if the resolution in that region is not sufficiently high. Thus, the resolution requirement in the upstream separation region is larger for the Hybrid-SA model than for DES97.

Within the jet plume, the velocity statistics predicted by the DES97 and Hybrid-SA simulations were nearly indistinguishable. The most significant difference was found in the separation region upstream of the injector. Separation occurred upstream of the experimental measurement in the DES97 simulation, as expected. The result was a poorly predicted wall-pressure profile. The Hybrid-SA model maintained the RANS behavior of the inflow profile and resulted in improved prediction of the separation location and wall pressure. This result demonstrates the utility of the Hybrid-SA model's ability to have side-by-side regions of pure RANS and wall-modeled LES.

Simulations of reacting flows with hybrid RANS/LES

Mixing of air and fuel inside of a scramjet combustor is a highly unsteady process. Intermittent pockets of fuel in shear layers between fuel and air streams can travel far downstream before becoming well mixed. Shear layers also can entrain large pockets of pure air, and time-averaged measures of fuel-air mixing often overestimate the level of instantaneous mixing. Current RANS models are not capable of capturing this important feature of the flow. For this reason, our approach is to simulate the mixing and combustion process with large eddy simulation (LES) that allows a large portion of turbulent flow scales to be resolved.

Pure LES inside a scramjet combustor is not feasible because the flow is wall-bounded and because of the high Reynolds numbers associated with this type of flow. Thus some type of wall modeling is necessary. To make the problem tractable for a realistic combustor, one also must be efficient in the use of LES regions. As much as possible, LES should be used only where necessary, limiting the flow regions where high grid resolution is needed. In regions where the flow is attached and where mixing and combustion are not occurring, RANS is preferred, as these regions are where RANS performs well and requires a lower grid resolution than LES. What is required is a hybrid RANS-LES method that will allow side-by-side regions of pure RANS and wall-modeled LES (WMLES).

The experiments of Ben-Yakar *et al*. (2006) provide a starting point for simulating the reacting case. In the experiments, high-speed schlieren images and planar laser induced fluorescence (PLIF) of OH radicals provide information on the instantaneous structure and ignition characteristics of a sonic hydrogen jet injected normally through a circular injector into a supersonic freestream. The freestream is air at Mach 3.38, and has a static temperature of 1290 K and a static pressure of 0.32 atm. These conditions correspond to combustor enthalpy conditions of Mach 10 flight. Hydrogen is injected through a 2 mm hole located 50 mm from the leading edge of a flat plate. The jet-to-freestream momentum ratio is $J = 1.4$.

The grid used for the simulation of the configuration of Ben-Yakar *et al*. contains 203 cells per d^3 in the high-resolution core away from the injector port, with d the injector diameter. The domain extends 5.7 d upstream and 16 d downstream of the injector. The low-resolution regions outside the high-resolution core extend to 7.6 d and 9 d in the spanwise and wall-normal directions. The grid is stretched to the wall containing the injector such that the first cell is within one wall unit. The resulting grid contains 14,781,200 cells.

Simulations were run on 200 cores of a 2.2 GHz dual-core Opteron cluster. The time step was chosen such that the local CFL number for cells inside of the jet plume was less than one. At the time step chosen, approximately 68 iterations are required to compute one flow time based on the jet exit diameter and freestream velocity. About 140 of these flow times can be computed in 24 hours.

Fig. 20 shows two instantaneous OH-PLIF images from the experiment, as well as two representative instantaneous images from the simulation. In the experimental images, a thin and nearly unbroken filament of OH radicals is seen, which starts very near the upstream edge of the injector and remains visible across the entire field of view. This result indicates that conditions for combustion are met and autoignition is achieved. Simultaneous schlieren and OH-PLIF images reveal that the filament lies on the boundary of the shear layer between the freestream and hydrogen gases.

The freestream gas immediately upstream of the injector is slowed considerably after passing through a strong bow shock caused by the presence of the jet plume. The gas of the jet plume itself is traveling at very high speeds due to the expansion it experiences as it exits the injector port. The velocity difference between these two regions of gas causes the formation of Kelvin-Helmholtz circumferential rollers that wrap around the jet shear layer. It is these large, coherent structures that cause the OH filament to wrinkle and fold upon itself.

The simulation images presented in Fig. 20 indicate behavior that is qualitatively very similar to that seen in the experiment. The presence of OH indicates that the 7 species chemical mechanism used can capture autoignition at these conditions. The signal is highest (indicated by yellow and white) on the windward side of the jet plume before the jet is turned fully in the downstream direction. Downstream of the injector location the signal level is reduced and the filament

becomes more diffuse; however, the experimental images do not provide a quantitative measure of the OH concentration, so we can not determine if the amount of OH produced in the simulation is at the same level as the experiment. The simulations also demonstrate that the large shear-layer structures are being captured.

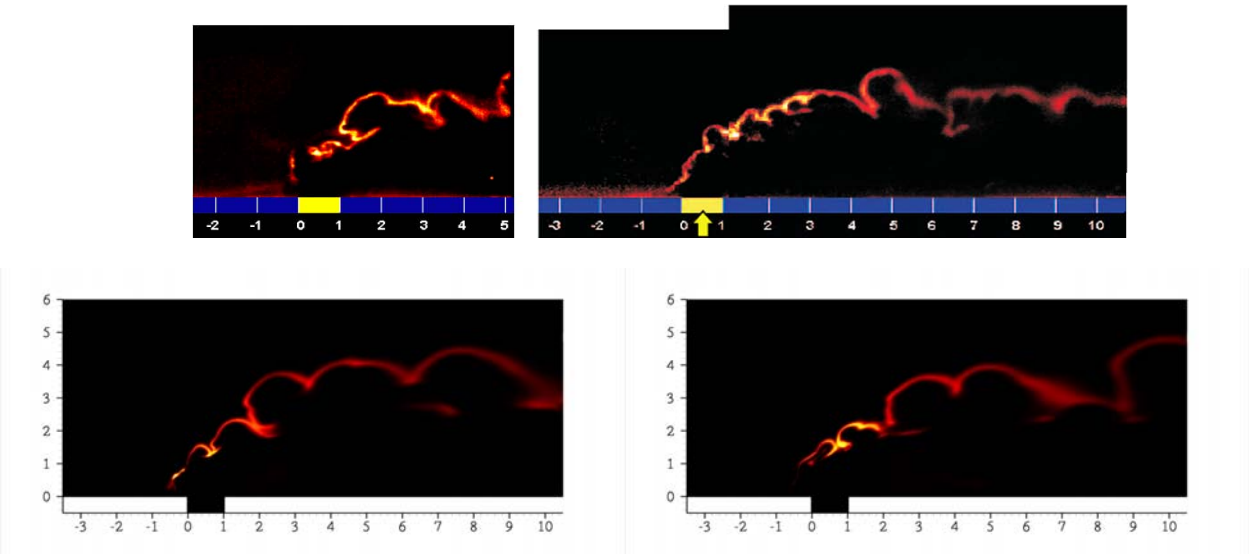

Fig. 20. Experimental OH-PLIF images (Ben-Yakar *et al.*, top) and simulation OH mole-fraction contours (bottom) across center line of jet plume.

To understand how the methods developed perform in realistic scramjet combustor geometries, configurations for which experimental data are available were simulated. The first such configuration considered is that of Tedder *et al.* (2005). In this experiment, a model scramjet combustor, referred to as the SCHOLAR model, is connected to the nozzle of a combustion-heated, supersonic facility. Vitiated gas from the heater is accelerated through a Mach 2 nozzle before entering the combustion chamber at the test conditions of 926 K (static temperature) and 101 kPa (static pressure). Hydrogen is injected through a normal, circular injector located 4.6 injector diameters downstream of a backward facing step 1.02 injector diameters high. The total H_2 temperature is 290 K, and the total pressure is 1.35 MPa. The target equivalence ratio for the combustor is 0.7.

For the simulations of the SCHOLAR combustor that involve the combustion of hydrogen with oxygen, finite-rate chemistry is coupled with the fluid solver. The chemical mechanism used relies on the seven-species, eight-reaction mechanism of Evans and Schexnayder (1980). At present, a subgrid turbulence-chemistry interaction model has been discussed as part of possible future collaborative work with Caltech but is not part of the simulation. Reaction rates are evaluated using the resolved quantities of the simulation. It is hoped that the effect of such a model on the simulation results will be part of future work.

The grid used in this simulation was constructed completely out of hexahedral cells using the commercial grid generation software GridPro. The grid extends from 0.1 m upstream of Plane 1 to Plane 7 in the streamwise direction, such that the length of the combustor being simulated is more than 1.2 m. The domain extends to the combustor walls in the spanwise and normal directions. In the vicinity of the injector port the grid contains approximately 163 cells per d^3, with d being the injector diameter. The grid becomes much finer near the exit of the injector port, with approximately 643 cells per d^3 in that region. Grid resolution decreases downstream such

that near Plane 7 there are approximately 53 cells per d^3. The grid is stretched to the walls of the combustor such that the first cell is within one wall unit. The resulting grid contains 40,130,555 cells.

Simulations were run on 600 cores of a quad-core AMD Opteron cluster. The time step was chosen such that the local non-dimensional time step, or a CFL number (Courant-Friedrichs-Lewy number, defined as the grid spacing divided by the local characteristic flow speed) for cells inside of the jet plume was less than one. At the time step chosen, approximately 118 iterations are required to compute one flow time based on the jet exit diameter and freestream velocity. A flow time based on the 1.11 m distance between Planes 1 and 7 and the freestream velocity corresponds to 149 jet-flow times and will be referred to as the domain-flow time. Approximately 66 jet-flow times or 0.44 domain-flow times, can be computed in 24 hours on the cluster used.

The simulation is started in a pure RANS mode to allow the mass flow through the injector, as well as other flow structures, such as shocks and the recirculation behind the step, to establish quickly. This initial simulation is run for approximately 0.18 domain-flow times. From the end of the RANS initialization, the simulation then is run using the DES97 formulation because of the nature of the hybrid-SA model. The hybrid-SA model is designed such that RANS behavior is maintained in regions of the grid where no LES content exists and the eddy viscosity is high, even if the grid is fine enough to support the LES spatial content. Thus, the model sees the initialized RANS flow with no LES content and high eddy viscosity, and switches to LES mode in regions where it should, such as the jet plume. The simulation is run in DES97 mode for an additional 0.31 domain flow times. This time is long enough for the eddy viscosity to drop and for LES content to develop in the jet plume and the recirculation region behind the step. The simulation then is run to completion using the hybrid-SA model. All results showed for the SCHOLAR combustor used the third-order upwind-biased inviscid flux reconstruction. Future work will focus on applying the low-dissipation numerics to this case.

Instantaneous images that superimpose Mach number contours with OH mole-fraction contours are shown for several instants in time in Fig. 21. Mach number contours reveal the turbulent flow field in the wake of the backward facing step and jet plume. The flow field downstream of the jet plume is found to be highly unsteady, even though the inflow condition is a steady-state RANS profile. The unsteadiness is caused by the interaction of the resolved turbulent structure in the low-speed separation region behind the step and the jet shear layer. Also visible in the figure are the complicated, three-dimensional shock structures that propagate down the length of the combustor, as discussed below. The OH contours show how the jet plume structures completely fill the combustor from top to bottom for most of the length of the combustor.

The 7-species chemical mechanism used for this simulation captures autoignition of the hydrogen jet. In the initial stages of the flow, OH is not seen along the tunnel centerline until many injector diameters downstream of the injection location. Some OH is formed in the jet shear layer but only in small intermittent pockets. The OH seen in the wake of the injector on the top wall in the top image of Fig. 21 originates from the combustor side walls just downstream of the step. A horseshoe vortex that wraps around the injector transports hydrogen to this region, where it mixes well with the freestream gas and ignites. It then is transported to the center of the tunnel by the counter-rotating vortex pair (CVP) formed by the jet plume. The CVP lifts this hot, reacting gas off the tunnel wall and mixes it with the rest of the jet plume.

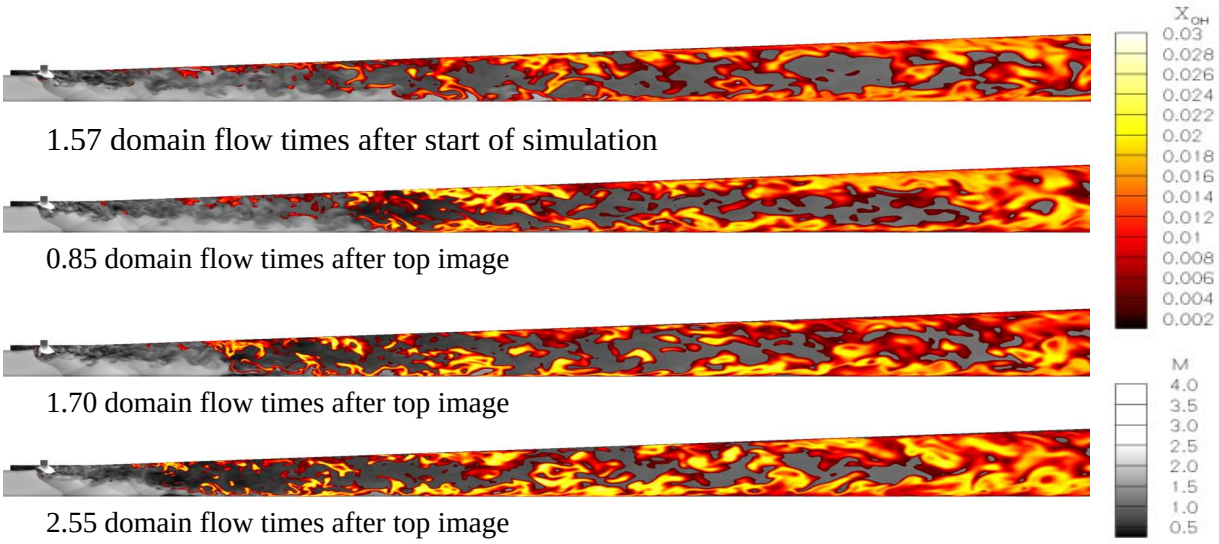

Fig. 21. OH mole fraction contours (color) superimposed on Mach number contours (gray scale) on the SCHOLAR combustor centerline.

The simulated flow is very similar to that in the top image of Fig. 11 for the first 1.8 domain flow times of the simulation. At this time the flow begins to become thermally choked about 48 injector diameters downstream of the injector port. The pressure increases and flow speed decreases from initially supersonic to subsonic speeds. The adverse pressure gradient in this region separates the boundary layer from the walls of the combustor. Then the high pressure, low-velocity front begins to propagate in the upstream direction. The combustion front is clearly visible in the two middle images of Fig. 21. The front propagates upstream past the injector and step, separating the flow and causing a complex shock-boundary layer interaction flowfield well upstream of the step, as seen in the bottom image of Fig. 21. After initially reaching this point, the separation recedes back downstream to the injection location. The separation region then oscillates between the injection location and a location upstream of the step several times. After 11 flow times, the flow appears to establish itself with the separation region upstream of the step. The separation region remains in the upstream region for more than a full domain flow time but then begins to recede downstream and oscillate back and forth again.

In the initial stages of the flow, the hybrid-SA model maintains the RANS boundary layer profile on the combustor walls upstream of the step. After the step is reached, the model senses the massive separation and promptly switches to the WMLES mode on the wall containing the injector. The WMLES mode is maintained along the entire length of the injector wall downstream of the step. On the other walls RANS behavior is maintained for a considerable downstream distance, until the point where LES content from the jet plume begins to interact with the walls. This simulation demonstrates the utility of this hybrid method for complex flows in realistic geometries, such as the SCHOLAR combustor, as no zonal information had to be supplied to the model in order to get the desired behavior; however, once the flow becomes thermally choked and the boundary layer separates from the walls, the model switches to the WMLES mode downstream of the separation on all of the walls. The intention was for the RANS boundary layers to be maintained on the walls not containing the injector. This switch to the WMLES mode on the injector walls is likely to have consequences in terms of the prediction of skin friction on the combustor walls and deserves more investigation in the future. Additional comparisons with the CARS data (Tedder *et al*. 2005) and the measurements of wall pressure are presented in Peterson and Candler (2008).

Initial results from the simulations of two reacting turbulent flows are promising. The simulation of the SCHOLAR combustor demonstrated that the flow inside a scramjet combustor can be very slowly evolving. Thus, an efficient solver with implicit time integration is needed. An expansion-ramp combustor based on the experiments at Caltech also was simulated. These highly preliminary simulations were performed using a low-dissipation, kinetic energy conserving flux evaluation method. The increase in the range of turbulent length scales resolved with this method, as compared to an upwind-biased scheme, was demonstrated. Further work is needed in the simulation of the combustor section, including grid resolution studies and the inclusion of a subgrid turbulence-chemistry interaction model.

Summary and conclusions

The MURI program enabled a number of important findings and advances in the simulation of scramjet flows. This report presents only a brief summary of the work conducted at the University of Minnesota. Our key conclusions are:

- The role of numerical dissipation in the simulation of scramjet combustor flows cannot be over-emphasized, as also concluded as part of the Caltech work. Great care must be taken to reduce the levels of dissipation, and conventional upwind flux methods are unlikely to be sufficiently accurate to produce reliable results on reasonable sized grids. Evolving low-dissipation methods may reduce the grid requirements, though these methods must be made more robust before they enter the mainstream of simulations.
- The hybrid RANS/LES approach investigated here has great promise. The most recent approach of using a RANS method to model the wall of an LES appears to be particularly interesting for scramjet flows. More work is required to make this approach more reliable and less sensitive to grid resolution and initialization.
- We strongly feel that the huge range of time scales in scramjets requires the use of an implicit time integration method to allow meaningful time steps to be taken. The SCHOLAR simulation requires many flow domain times to reach a quasi-steady state. Without an implicit method, it would be impossible to evolve the flow sufficiently far to understand its dynamics.
- A lack of validation-quality experimental data at scramjet conditions persists.
- Grid generation is an important aspect of simulating scramjet flows. Novel grid generation approaches using many small blocks of hexahedral elements is a potential approach to obtain high quality grids that use the grid points efficiently. Scramjet simulations are extremely costly and therefore the grid resolution must be placed carefully in regions where it is needed.
- The use of RANS to simulate scramjet flows should be phased out as soon as possible. Scramjet flows are dominated by unsteady turbulent motion, and it is misguided to think that RANS can capture these dynamics.
- Much remains to be learned about how to model chemistry-turbulence interactions in scramjet flows.
- The future is bright for the development of methods that can accurately predict scramjet-combustor flows. The combination of wall-modeled LES approaches, more efficient low-dissipation implicit numerical methods, novel unstructured grid generation approaches,

and the continuing increase in computational power offer the promise of reliable simulations of these flows in the near future.

Virginia Tech

The main efforts at Virginia Tech under this MURI focus on:

1) injection, mixing, ignition, and combustion in supersonic flows typical of scramjet combustors and
2) instruments for skin friction measurements in hot supersonic flows in the laboratory and on scramjet flight test vehicles.

This report first summarizes the results of experimental and computational studies of complex injectors conducted at a higher freestream Mach number than in most earlier work. The first injector was an aeroramp consisting of four flush-wall holes that induce vorticity and enhance mixing. For comparison, a single circular-hole injector angled downstream also was examined. Test conditions involved sonic injection of heated helium into a Mach 4 air cross-stream with average Reynolds number 5.77×10^7 per meter at a jet-to-freestream momentum flux ratio of 2.

Schlieren images and shadowgraphs were used to visualize the flow field. Aerothermodynamic sampling was accomplished with Pitot, cone-static, and total-temperature probes. Temperature was measured with a rake consisting of three tubes, each with a Type-E thermocouple inside. Helium concentration measurements were obtained using a sampling probe and gas analyzer designed specifically for use in supersonic flow. Isokinetic sampling was ensured in supersonic flow by swallowing the shock into the probe.

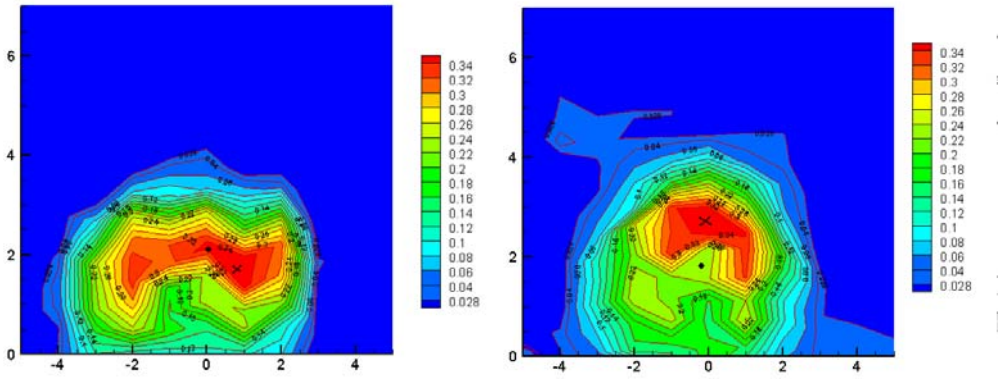

Fig. 22. Experimental helium mass fraction contours: Aeroramp (left) and single hole (right) located at x/d_{eq}=16.4, $\bar{q}$ = 2.

The numerical flow solver used for reference in this study was GASP v. 4.2 from AeroSoft, Inc.. All grids for the CFD studies were created using Gridgen v.13.3 from Pointwise Inc. The Wilcox (1998) *k*-ω turbulence model was used. Experimental results for the aeroramp injector and the single round hole comparator are shown in Fig. 22. A comparison of CFD predictions and the data for the aeroramp is presented in Fig. 23.

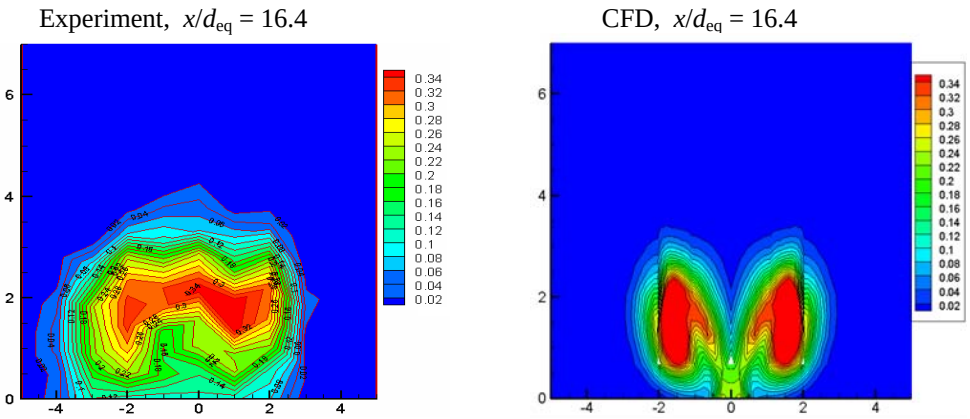

Fig. 23. Calculated helium concentration contours (left) in the x/d_{eq} plane of the aeroramp injector compared to experiment (right).

The goal of the next experimental and computational studies conducted was to determine the influence of shocks impinging near jet injection on fuel penetration and mixing. The jet/shock interaction is important for understanding scramjet combustors, since they typically have numerous shocks.

Heated helium was used to simulate hydrogen fuel. A single-hole circular injector angled downstream at 30 degrees was selected. A shock of modest strength ($p_2/p_1 \approx 2$) generated by a wedge above the surface, was impinged at three locations along the jet plume: x/d_{eq} = 2, 8 and 16, where d_{eq} is the effective diameter of the jet injector. See Fig. 24.

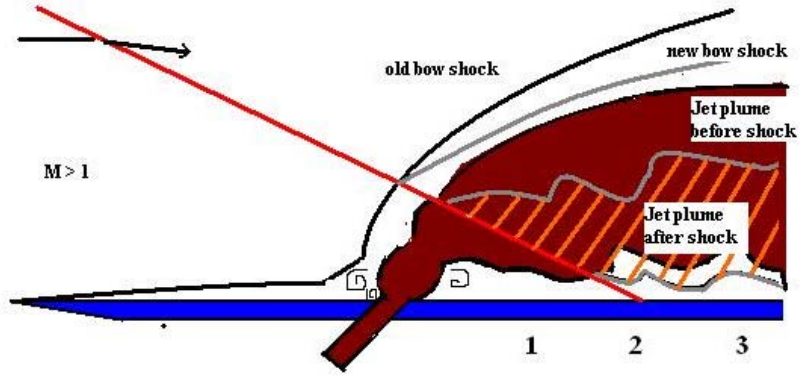

Fig. 24. Sketch of shock impingement on fuel jet studies

Some typical results are given in Fig. 25 in terms of contour plots of injectant mass fraction at a downstream station of x/d_{eq} = 16.4. The CFD predictions are in good agreement with experiment. This result is in contrast to the baseline case without shock impingement, where CFD underpredicted the observed rate of fuel dispersion.

One may postulate that the CFD is better able to capture the largely inviscid effects of the shock compared to the turbulence effects alone in the case without shock impingement. Second, the shock impinging just downstream of the injection station has a larger effect than those impinging further downstream, which is most likely a result of the larger density gradients in the jet plume near the injection station, which lead to stronger baroclinic torque effects.

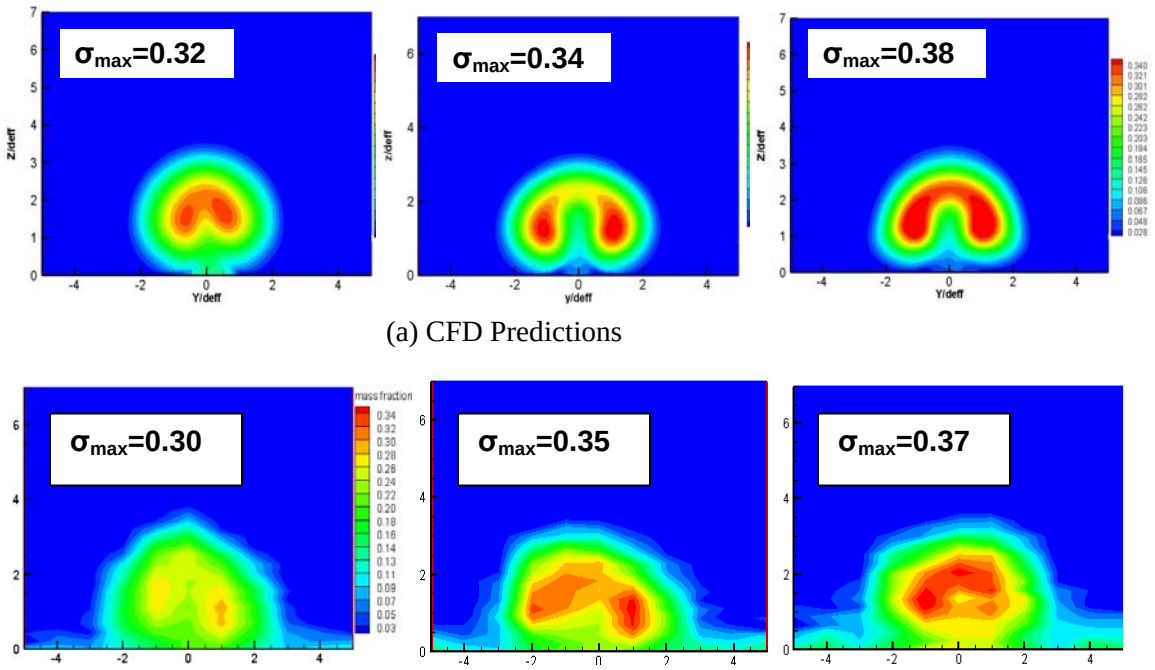

Fig. 25. Injectant mass fraction contours at x/d_{eq} = 16.4 for shock impingement at x/d_{eq} = 2, 8, and 16.

The main aim of the next injector studies conducted was to determine the influence of axial vortices passing near jet injection on fuel penetration and mixing. This interaction is important for understanding scramjet combustors, since they typically have numerous axial vortices from the inlet, struts, and/or other injectors.

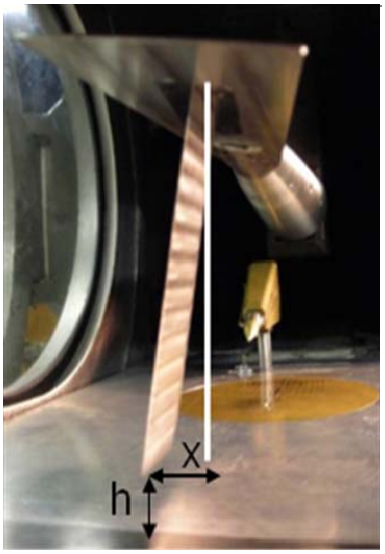

Fig. 26. Photograph of the vortex generator and sampling probe in the VT supersonic wind tunnel. The location of the vortex is defined by (x,h).

Heated helium was used to simulate hydrogen fuel. A single-hole circular injector angled downstream at 30 degrees was selected. An axial vortex was produced by an upstream double-

wedge wing, and the vortex strength was set to be typical of a vortex produced in an inward-turning inlet. Sampling probe measurements were utilized to determine the local helium concentration, and a special five-hole probe was used to document the flow. The setup in the supersonic wind tunnel can be seen in Fig. 26.

Some comparisons of the flow with axial vortices interacting with the jet plume in various locations are shown below in Fig. 27. The definition of the location of the vortex generator in relation to the jet injector is shown in Fig. 26. These results document the very large influence that the external axial vortices have on the basic jet flow development. Note the distortion of the jet plume and changes in jet penetration.

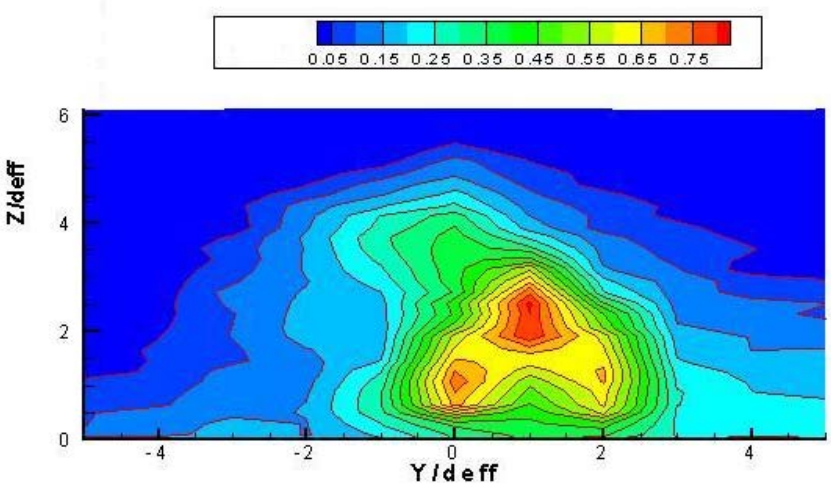

(a) Vortex generator at $x = 0$; $h = 2\ d_{eq}$.

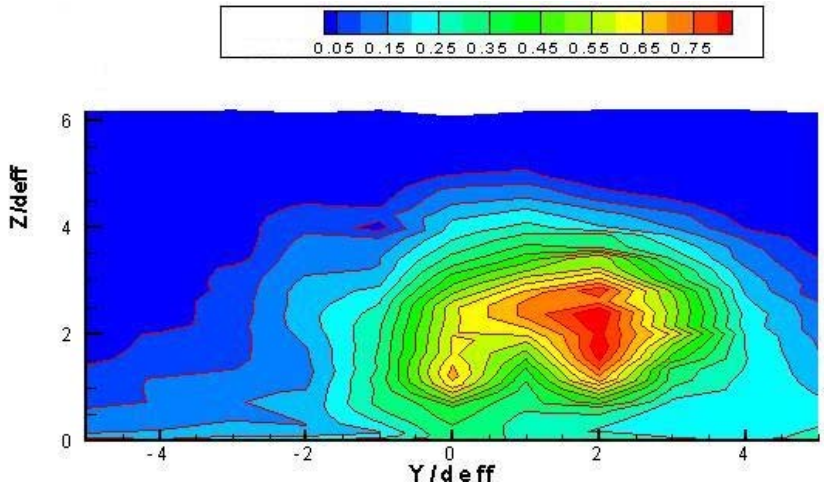

(b) Vortex generator at $x = 0$; $h = 1\ d_{eq}$.

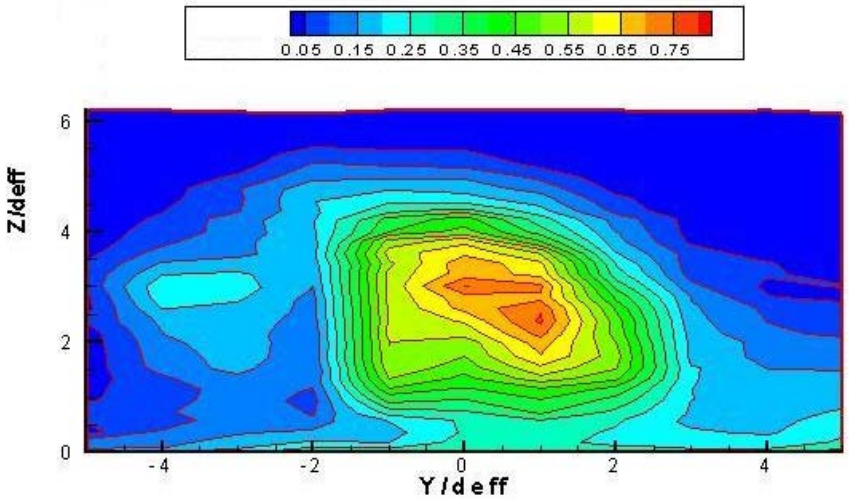

(c) Vortex generator at $x = 2$; $h = 2$ *deq*.

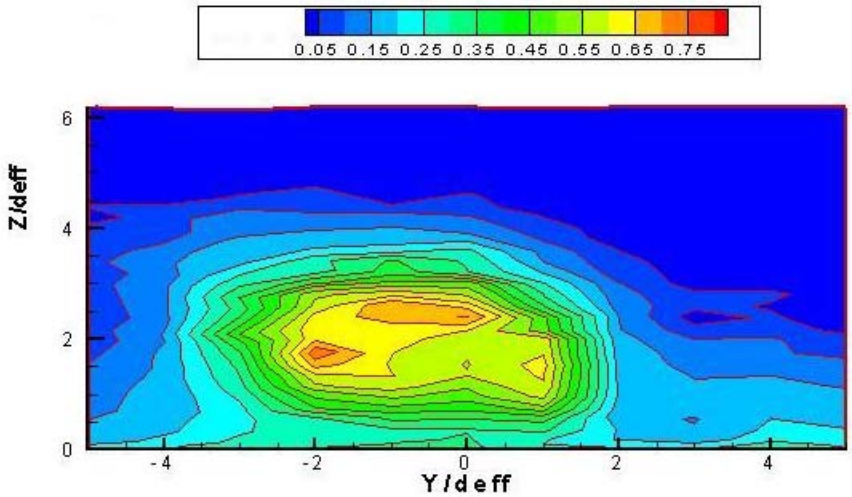

(d) Vortex generator at $x = 4$; $h = 2\ d_{eq}$.

Fig. 27 Injectant mass fraction contours at $x/d_{eq} = 16$, for various vortex generator locations.

Skin-friction measurements are necessary to determine aerodynamic force impact on vehicle performance, especially for high-speed, air-breathing vehicles. Direct and indirect methods are available to quantify skin friction, but only direct measurements eliminate the need for prior understanding of the flow. One such direct-measure gage uses a movable wall element or floating head. This element is connected to some sort of flexure. A cantilever beam version of this gage allows flexure to weaker wall shear forces while remaining stiff relative to stronger pressure forces normal to the head. The transduction system employs a four-strain gage configuration in two separate half-Wheatstone bridges to quantify and minimize the effects of shock impingement on the floating head which is critical to the successful application of these devices in scramjet combustors.

A skin-friction measurement device will experience acceleration, vibration, temperature, axial, moment, and shear loading. The design goal is to minimize or separate out these components while maximizing the sensitivity to shear loading. Minimizing the mass of the device and damping mitigate acceleration and vibration loads. Temperature effects arising from conduction

and radiation are minimal, as can be seen through experiment and finite-element modeling (FEM) results. The convective effects have been minimized in this design using very thin-walled bellows surrounding the sensor elements. Additionally, paired metal-foil strain gages in the half-Wheatstone bridge help mitigate thermal effects. Axial loading impact is minimized by beam stiffness in the axial direction. Additionally, the symmetric placement of strain gages on opposite sides of the beam allows for cancellation of purely normal forces leaving moment and shear loading. The relationship between shear and voltage output, as well as the relationship between moment and voltage output, is linear. By employing two separate half-Wheatstone bridges at different axial locations, the shear and moment loads can be separated.

The cross-sectional design of the beam was developed through a strain vs. frequency trade study using FEM. The strain had to be high enough to measure, but the frequency also had to be high to reach a steady state through impulsive loading with short tunnel run times, such as in the Large Energy National Shock (LENS) tunnel facilities. Unfortunately, a cross section that provides high strain is less stiff and has a lower frequency; therefore, a cross-section that balances these design requirements was chosen. Figure 28 shows the skin friction gage assembly. The head diameter is 0.25 in. Figure 29 (left) shows the strain gage locations along the beam. The opposite gage pairs are place symmetrically opposite of the visible pair. Figure 29 (right) also shows the expected compressive strain distribution from a 2000 Pa shear load.

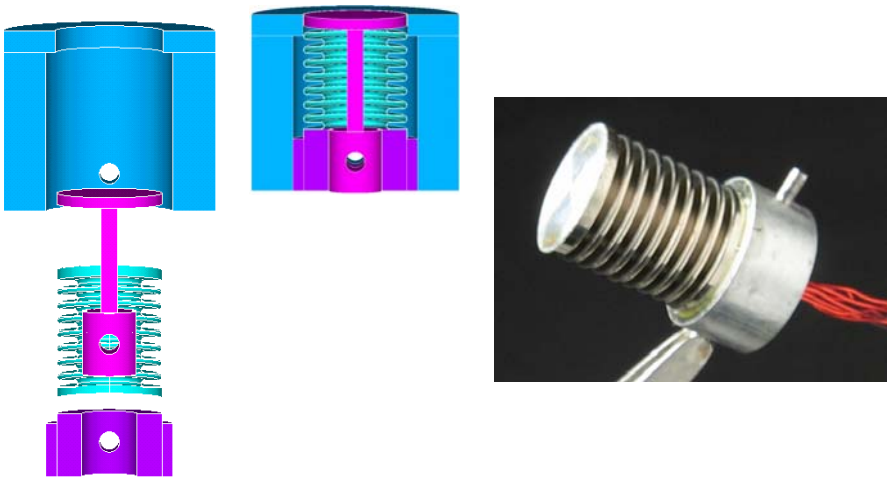

Fig. 28. Skin-friction gage assembly.

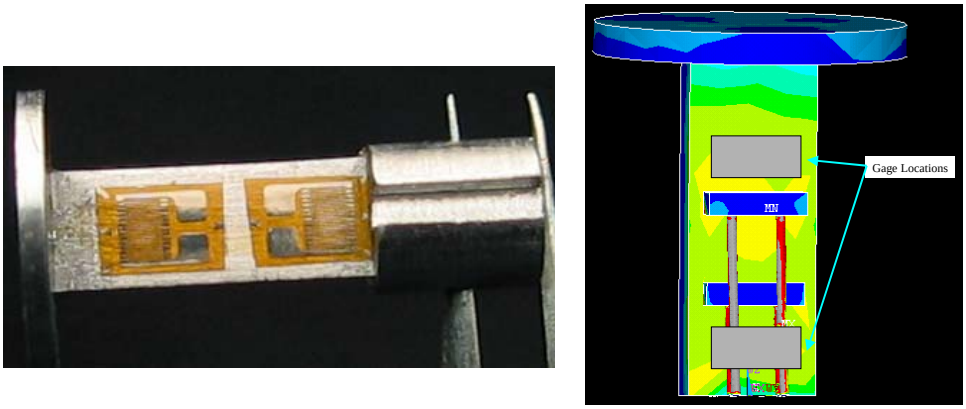

Fig. 29. Strain gage application (right). Compressive side strain distribution from a 2000 Pa shear load (right). FEM from ANSYS®.

University at Buffalo (UB)/CUBRC

During the MURI program, the University at Buffalo (UB)/CUBRC conducted experimental and numerical computation work that was integrated tightly with that of other members of the MURI team, as well as discussed with technical staff at the Air Force Research Laboratory. At UB, three doctoral students and one post-doc contributed to this program. UB also was engaged actively with students at both the University of Minnesota (U M) and Virginia Tech (VT). All of the experimental work conducted in this program either was published or is freely available in non-ITAR form and, as is standard practice at UB, is accompanied by complementary numerical results from UB and the MURI team members.

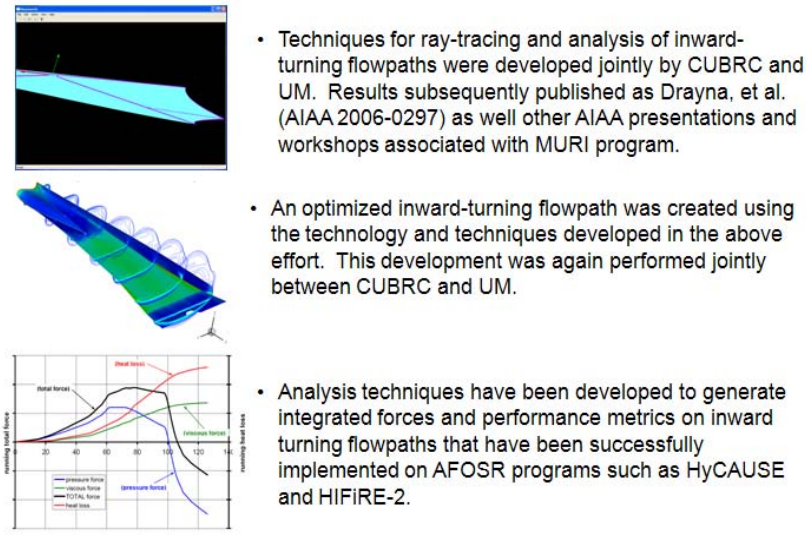

Fig. 30. Inward turning flowpath design and optimization efforts.

An example of such activities is shown in Fig. 31, where in the first year of the program there was an integrated activity to support the optimum design of efficient inward-turning inlets by the members of the MURI team.

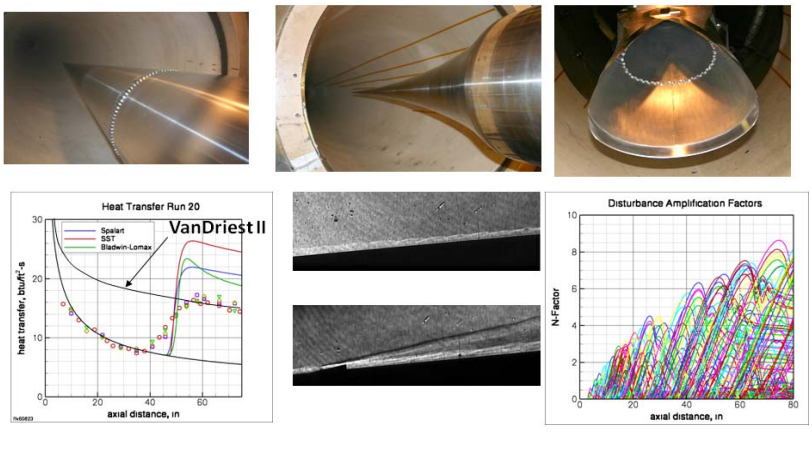

Fig. 31 Experimental and numerical studies of inlet boundary layers, including tripping

Boundary layer tripping is a key part of contemporary inlet designs, and UB, in conjunction with UM, conducted experimental and numerical studies on 2D and inward-turning inlets to develop techniques to predict trip performance and the subsequent development of the turbulent boundary layer accurately. Figure 32 shows examples of these studies. Techniques to predict transition onset, such as via the use of the University of Minnesota STABL code, also were explored.

A major objective of the experimental studies in the UB MURI program was to investigate mode switching and inlet starting. This was part of the MURI Broad Agency Announcement and re-emphasized in discussions with Dr. Tishkoff at AFOSR and key staff at the AFRL propulsion lab. The substantive experimental program conducted at UB involved sophisticated models and instrumentation employed to investigate the unsteady flow phenomena associated with turbine-to-ramjet mode switching and inlet starting of inward-turning inlets.

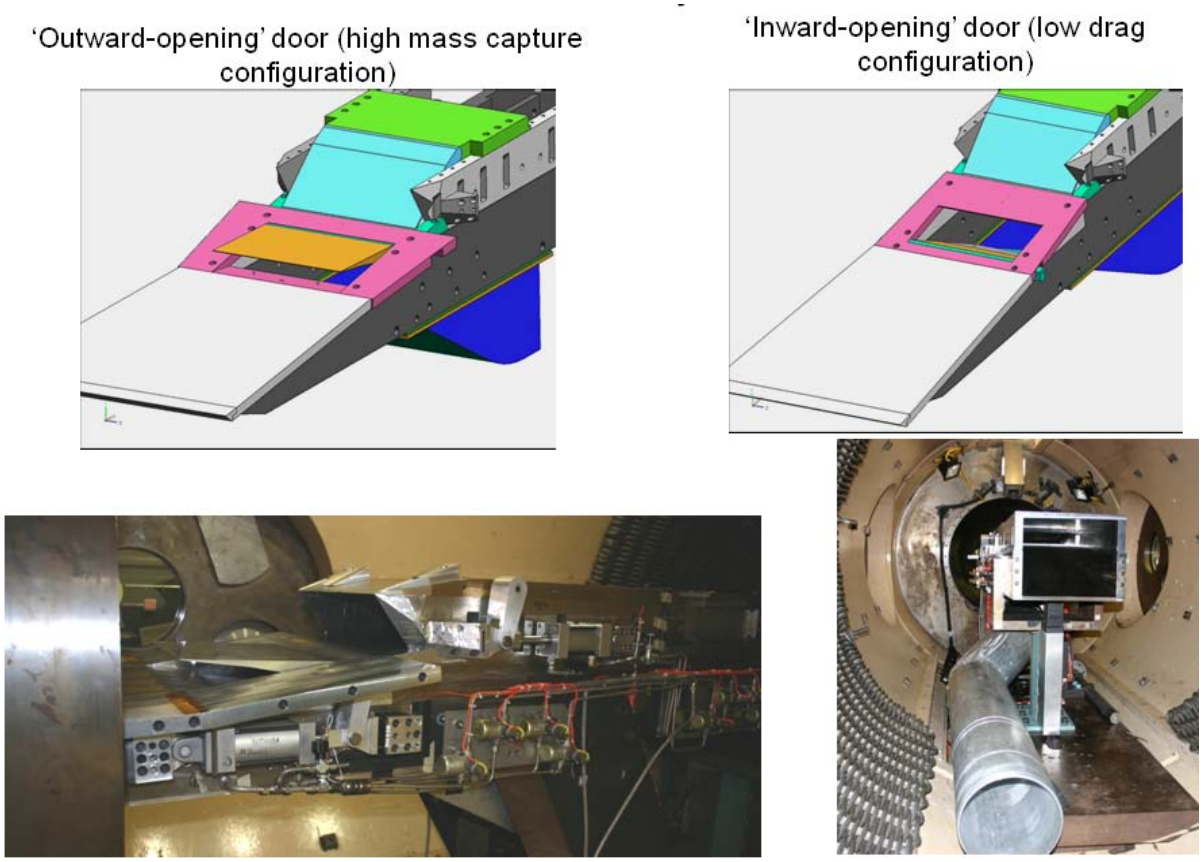

Fig. 32. Schematic showing the actual sequence of turbine and ramjet doors.

In this program two mode switching configurations of practical interest were employed. Inward- and outward-turning turbine door configurations coupled with an outward-opening scramjet door were employed in a full-scale flowpath typical of dual mode engines in the 10 to 20 lbs/sec scale, as shown in Fig. 32.

During the flowpath design and the experimental program, extensive numerical computations were undertaken. Some results are shown in Fig. 33 using the UM DPLR code to optimize inlet design and evaluate starting phenomena, particularly during turbine-door opening. Unique sets of time-dependent measurements, as shown in Fig. 34, were obtained throughout the engine to characterize the unsteady flow phenomena that ensue during mode switching.

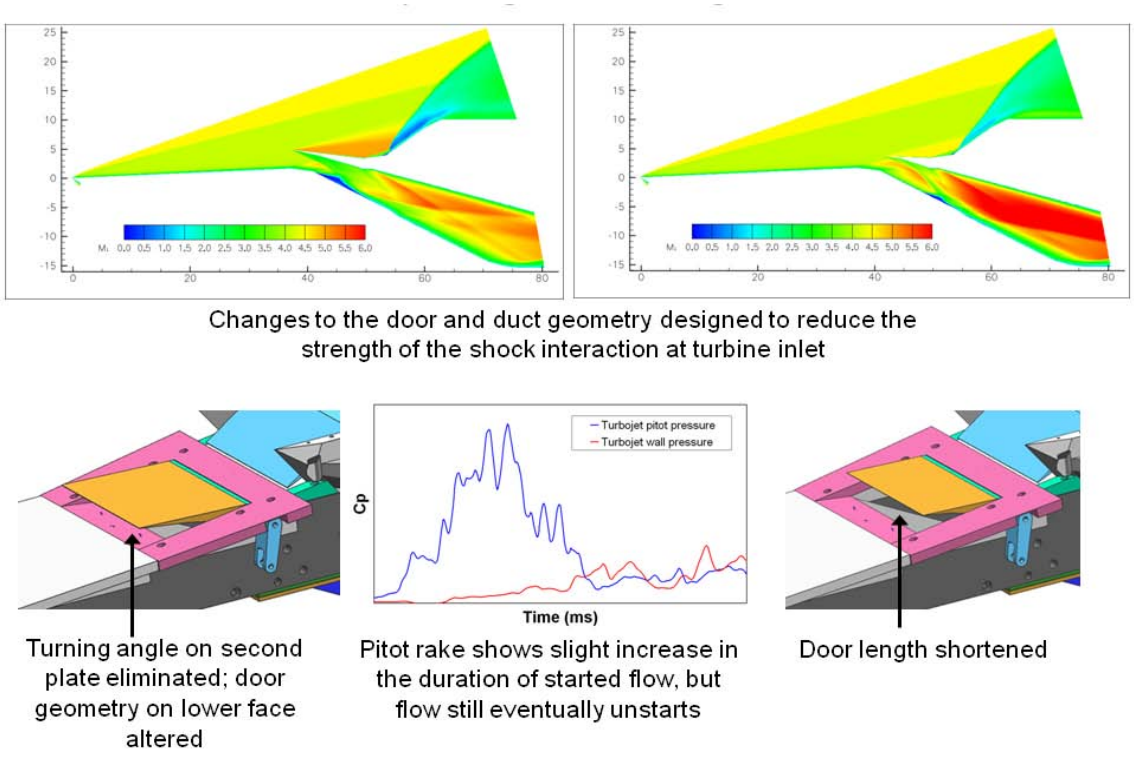

Fig. 33. Outward-opening door design iterations.

Of particular importance were measurements of unsteady shock-interaction phenomena that have a major impact on aerothermal loading.

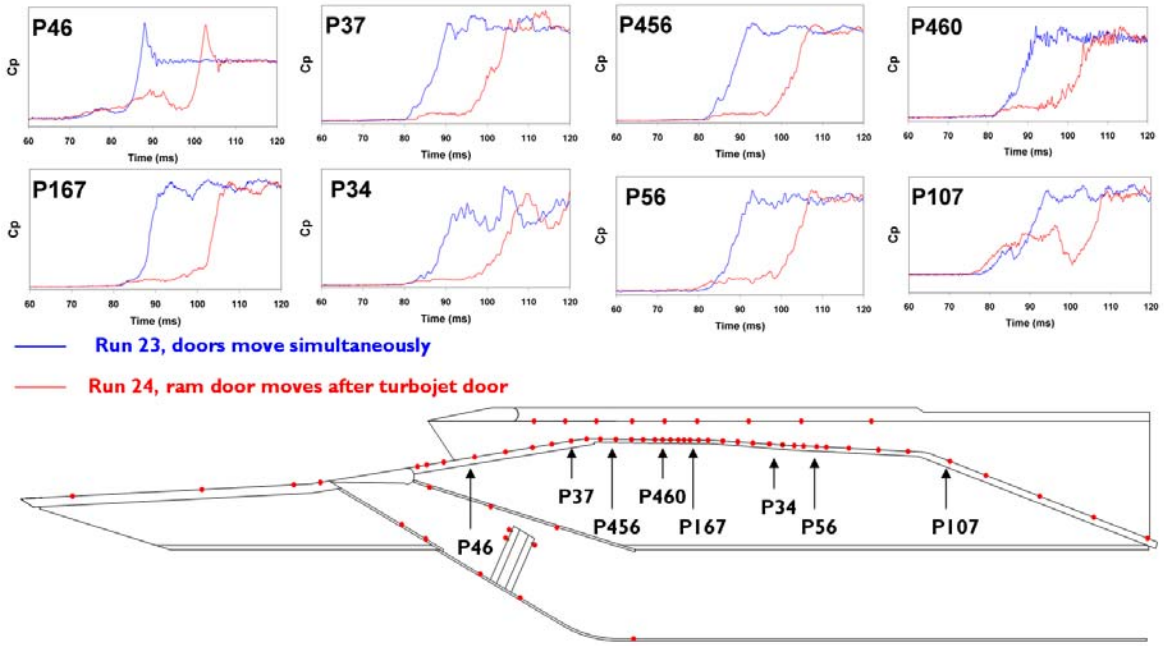

Fig. 34. Outward-opening door transient comparison, showing nearly identical startup process independent of turbine door motion

This data set, which has been shared with the MURI team and members of the research community, provides unique information with which to evaluate the numerical code performance. Initial numerical studies to examine the unsteady flow phenomena associated with starting doors on the inward-turning inlet were conducted by UM using their unsteady Navier-Stokes code. It was demonstrated that the key issue in starting-door design was associated with eliminating the extensive region of laminar-flow separation that enveloped the entire inlet.

The development of a successful inlet/starting door design requires that the boundary layer must be tripped on the inlet to obtain turbulent flow to minimize the extent of the separated region. Conventional inlet-starting mechanisms with "intelligent holes", etc. would not be effective in this situation. A start door configuration was designed and fabricated, as shown in Fig. 35, and implemented in the HyCAUSE inlet. In addition, we constructed a slide valve that, when closed, would unstart the engine completely. Tests were conducted with the opening sequence shown in Fig. 35 that produced detailed time-dependent measurements during studies of engine starting. These measurements were accompanied by computations typical of those shown in Fig. 36.

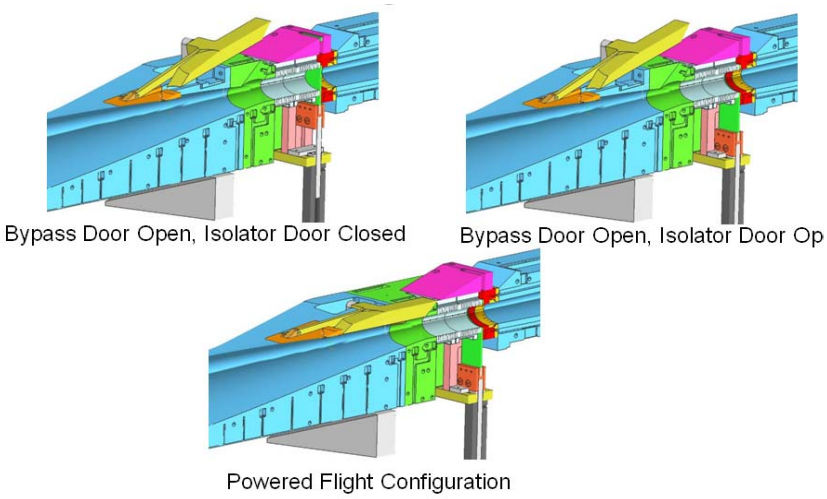

Fig. 35. Modification of HyCAUSE engine for starting-door studies.

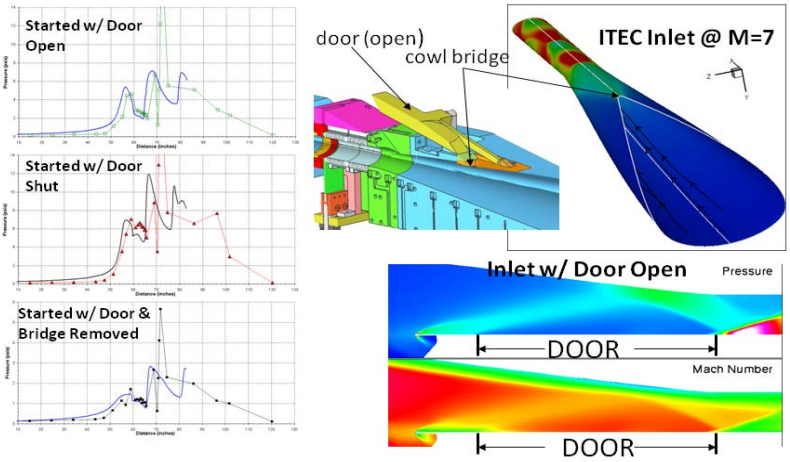

Fig. 36. HyCAUSE inlet-starting studies.

During the MURI program, continuous interaction occurred among members of the team on the design of injector systems used in the complementary experimental programs at UB studies and at VT. Simple cylindrical angled injectors were examined, together with diamond exit configurations, as well as the aeroramp configurations suggested by VT (Fig. 37).

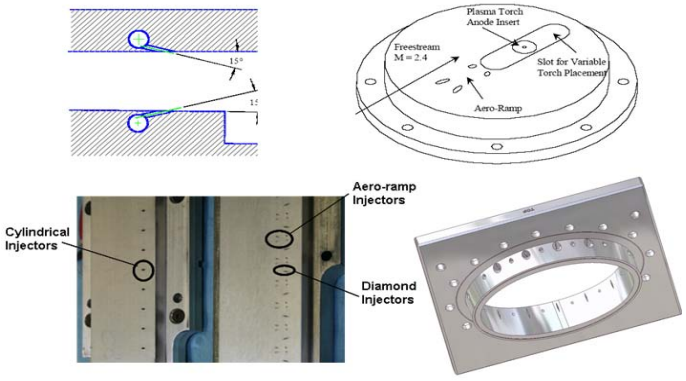

Fig. 37. Schematic of plume patterns from injector systems.

In the experimental studies, the performance of the Schetz aeroramps were compared with both cylindrical and diamond injector systems in both the 2D and axis-symmetric flowpaths. Again these studies were accompanied by numerical computation at VT, UB, and UM.

Major studies were conducted at both UB and VT to develop and test skin-friction gauges, as shown in Fig. 38, that would perform in the harsh environment of a scramjet combustor. At UB the experimental program centered on the development of a new high-frequency, high-load skin friction gauge using piezoelectric-sensing elements. To perform accurately in the combustor environment required a design that would accommodate the acceleration and pressure loads experienced in the engine. Following the design phase of the effort, initial flat-plate experiments were conducted to obtain local conditions that simulated the skin friction loads that would be experienced on the inlet and combustor of a full-scale engine at Mach 6 flight conditions. Following the successful completion of these studies, we installed gauges in the full-scale flowpath that was employed in the mode-switching studies. Severe vibrational loads in the combustor environment resulted in unsatisfactory measurements. It is hoped that the difficulties experienced will be resolved in future studies with modifications to account for the unsteady aerothermal loads.

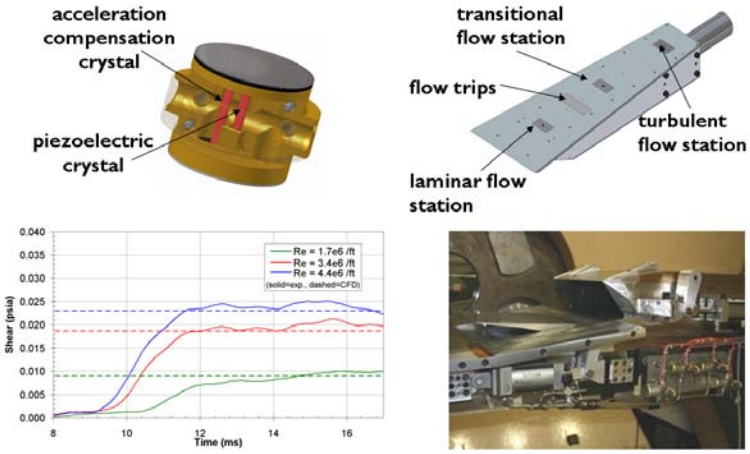

Fig. 38. Development and application of high-load skin friction instrumentation for scramjet combustor measurements

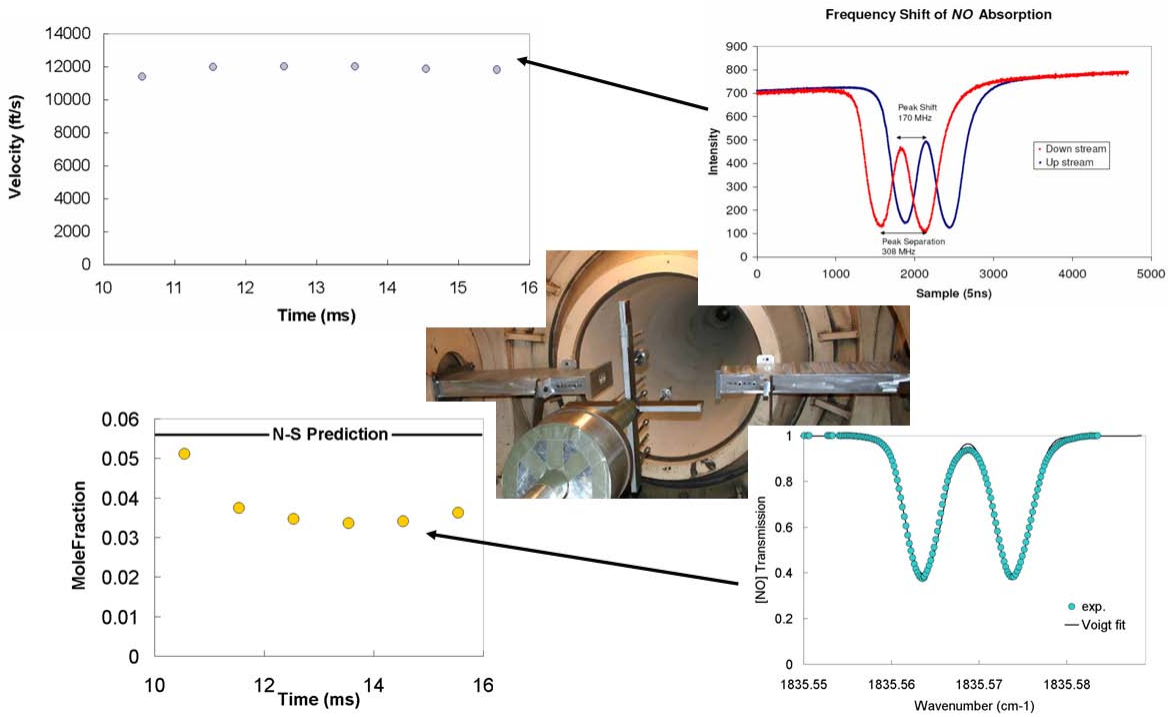

Fig. 39. Nitric oxide (NO) measurements in freestream preceding Mach 10 scramjet tests in LENS I.

In conjunction with the UM simulations and with technical assistance from AFRL, UB improved the nonintrusive measurement techniques to evaluate the freestream conditions and measure the composition of the reacting flow in a full-scale HyCAUSE combustor run at simulated flight conditions.

During our MURI studies to determine the freestream properties, accurate measurements of freestream velocity and NO concentration were obtained using laser-diode absorption spectroscopy. As illustrated in Fig. 39, measurements of freestream velocity were in excellent agreement with the Navier-Stokes predictions; however, the predictions of NO in the freestream were a factor of 2 larger than the measurement values.

Significant improvements also were realized in algorithms to obtain temperature and water vapor concentration measurements from the tunable diode laser (TDL) Zolo tomography system; however, the new results showed water concentration levels that differed significantly from those predicted by the CRAFT numerical code, as illustrated in Fig. 40.

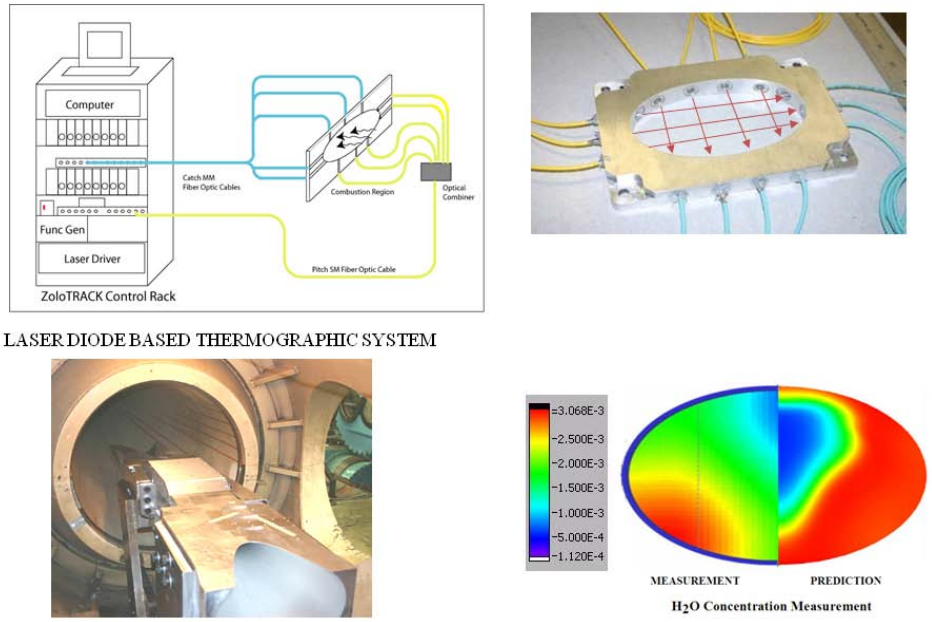

Fig. 40. Schematic of the TDL tomography system and software.

In a complementary study supported by the MURI program an infrared radiometer was developed (Fig. 41) to estimate temperatures in the HyCAUSE combustor. While there are significant issues with the interpretation of the data obtained with this system, it provided valuable insight into the combustor flowfield. Again, there was significant discrepancy between numerical predictions and temperature measurements in the combustor region. Measurements made at this time with the intrusive total enthalpy probes were inconclusive because of questions associated with the turbulent nature of the boundary layer over the probes.

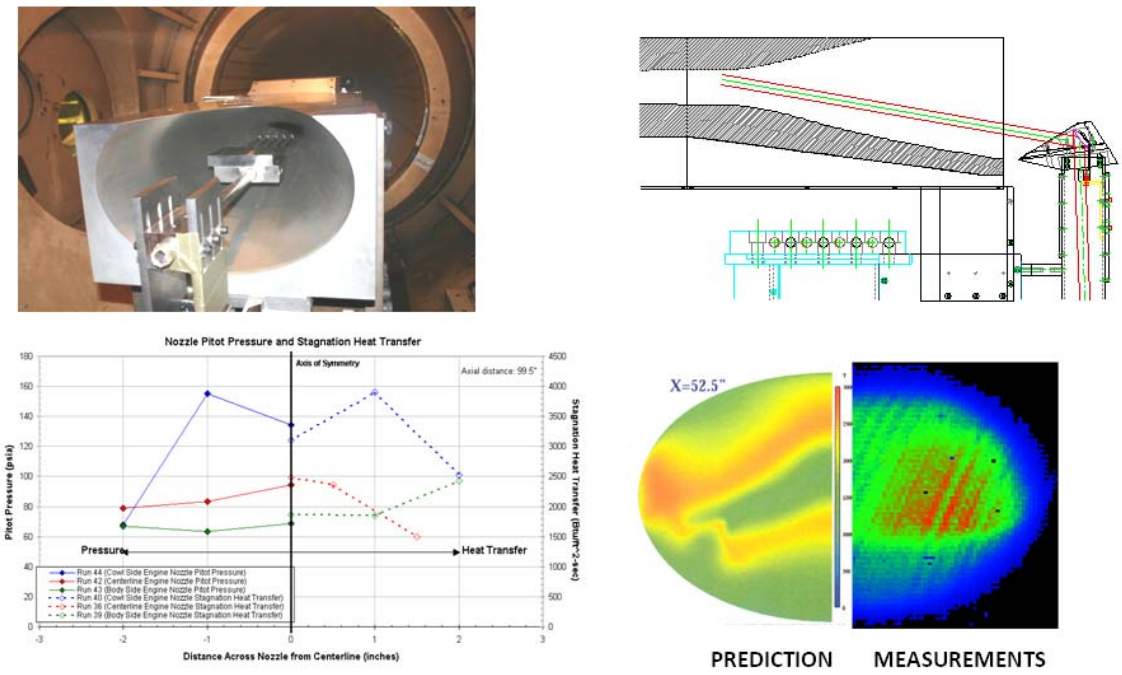

Fig. 41. Survey rake and infrared measurements.

A major addition to the program, relative to that initially proposed, was measurements to assess the effect of vitiation on the performance of a full-scale flowpath operated at Mach 6 flight conditions. Because most of the development testing associated with scramjet performance is conducted in vitiated air facilities, such as the 8 ft HTT and APTU facilities, the effect of vitiation is an important issue that has not been addressed directly in full-scale testing at flight conditions. As a part of the MURI program, the LENS II facility was modified by constructing a system to add vitiants to the flow. This capability was used to compare combustion in a full-scale flowpath for both hydrogen and ethylene fuels. Measurements first were made in the freestream of the tunnel to validate the vitiated composition of the flow (Fig. 42). Measurements then were made in both the clean environment and the vitiated flow to compare combustion performance, as shown in Fig. 43. While there were differences in the ignition process for the hydrogen engine, the final pressure was found not to be influenced significantly by vitiation; however, during the limited testing of the hydrocarbon-fueled engine, it proved infeasible to ignite the fuel in vitiated flow. This last finding presents a major concern and should be investigated in tests with a full-scale flowpath as soon as possible.

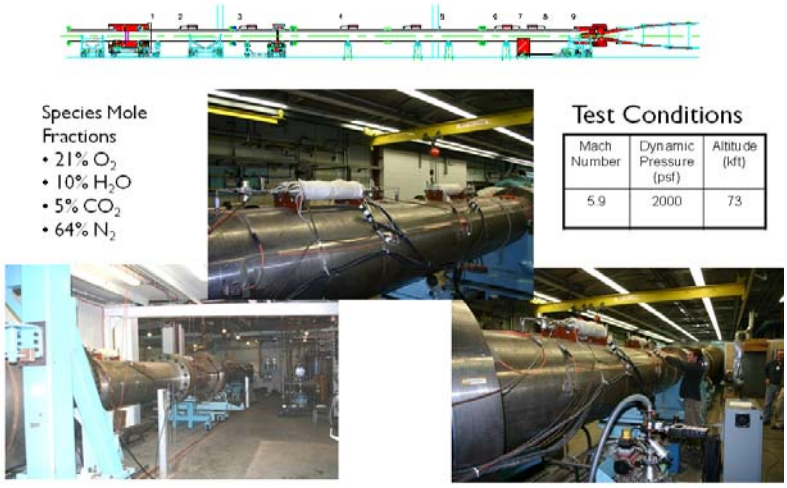

Fig. 42. System to add vitiants to tunnel reservoir

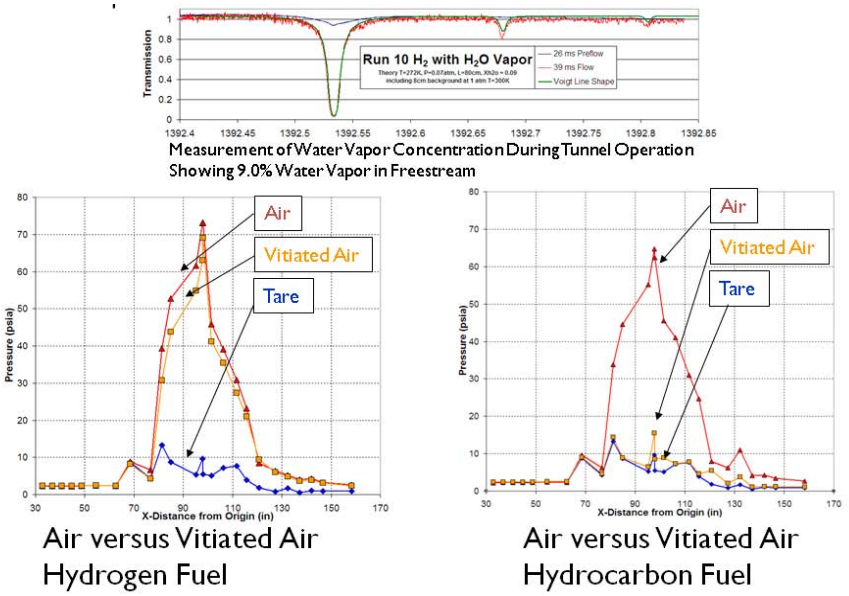

Fig. 43. Comparison between air and vitiated air operation in LENS II.

During the final two years of the MURI program, and in conjunction with technical input from other members of the MURI team and staff members of the AFRL Propulsion Lab, UB designed and constructed a simplified combustion duct with which to obtain fundamental data on mixing and combustion with simple injector systems tested at flight-duplicated pressure and enthalpy conditions. The UB program objectives for the experimental studies to be conducted with this apparatus are listed in Fig. 44. This design was drawn in part from the slightly more complicated HIFiRE-2 configuration, also shown in Fig. 45, and detailed computations to obtain a well-defined flowfield in the combustor. The combustion duct was constructed and highly instrumented during the MURI program, and initial studies were conducted initially at HIFiRE-1 conditions.

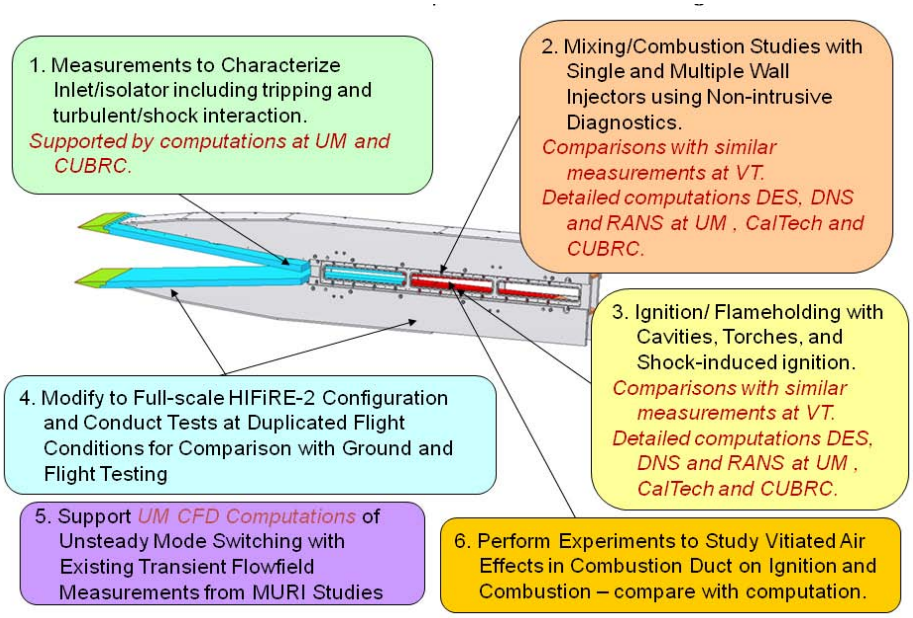

Fig. 44. Major objectives of experimental studies with the combustor duct model to generate fundamental data on injection, mixing, and combustion in clear air at duplicated Mach 6 to 10 flight conditions.

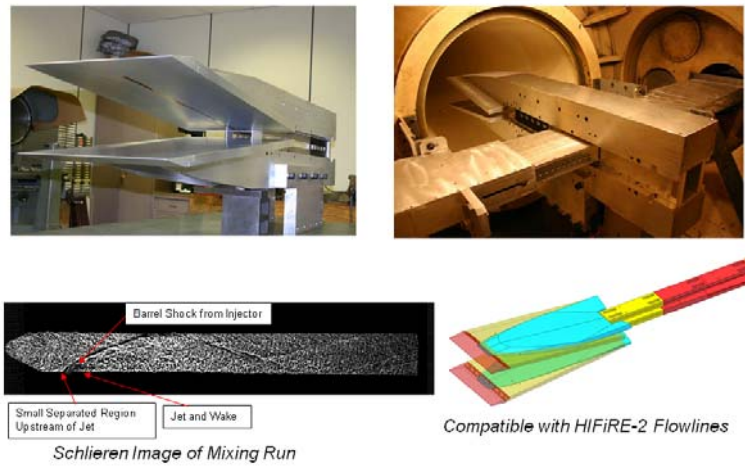

Fig. 45. Code-validation studies of mixing and combustion in the CUBRC LENS I facility at duplicated Mach 7.2 flight conditions.

Numerical computations with the UM DPLR code demonstrated a significant 3D shock structure in the isolator section, as shown in Fig. 46; however, as illustrated, the measured centerline pressure distribution was in reasonable agreement with the calculations accounting for the 3D nature of the flow.

The measurements shown in Fig 47 demonstrate that the trips on the inlet forebody were fully effective in transitioning the boundary layers to turbulence. For this geometry, the shock interaction patterns and peak heating and pressure levels in the isolator and combustor are accurately captured by the CFD predictions. Good agreement with CFD predictions has been difficult to obtain on inward turning and asymmetric planar geometries because of shock boundary layer interactions on those more complex inlets.

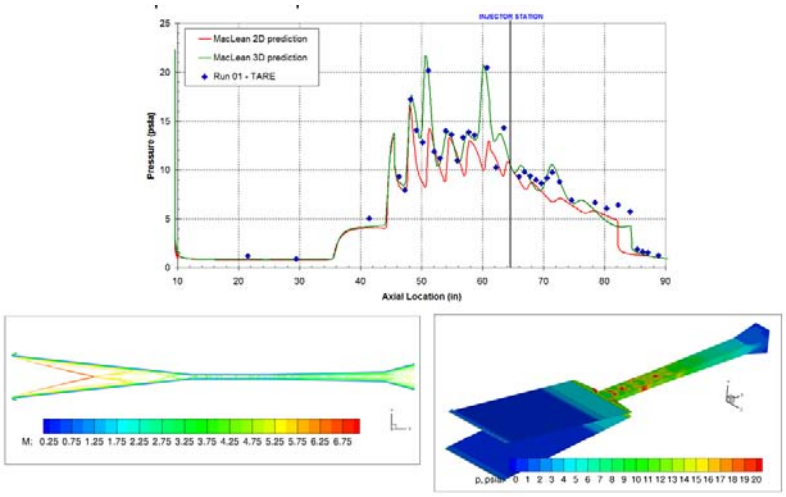

Fig. 46. Comparison of experiment and CFD for tare condition.

Based on our initial results, the flow quality in this experimental apparatus would provide fundamental experimental data on ignition, mixing, and combustion and would prove invaluable in evaluating the models of turbulence in regions of shock boundary layer interaction, fuel injection and mixing, ignition and flameholding, and combustion that would be available to university researchers developing numerical codes to describe these flows.

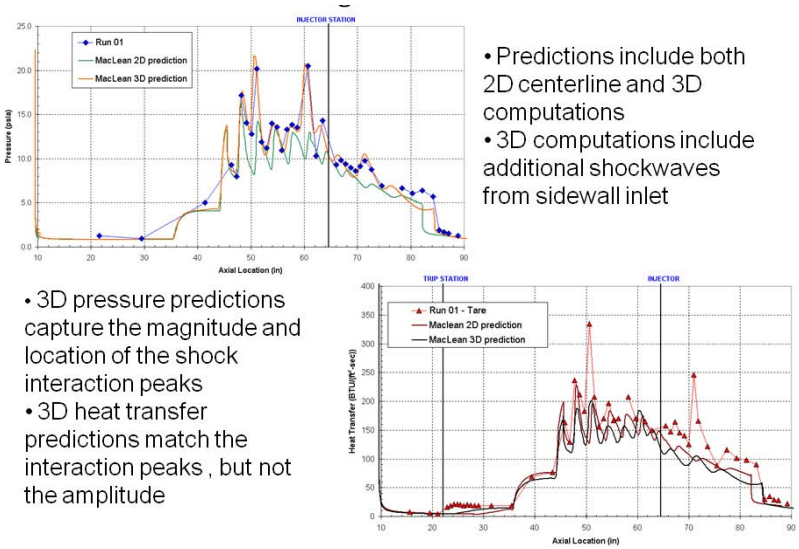

Fig. 47. Comparison between experimental results and predictions using the U of M DPLR code.

References

BARBER, M.J., SCHETZ, J.A., ROE, L.A., 1997 Normal, Sonic Helium Injection Through a Wedge-Shaped Orifice into Supersonic Flow, *J. Propulsion and Power*, 13(2).

BEN-YAKAR, A., M. G. MUNGAL, AND R. K. HANSON 2006 Time Evolution and Mixing Characteristics of Hydrogen and Ethylene Transverse Jets in Supersonic Crossflow. *Physics of Fluids, Vol. 18.*

BERGTHORSON, J.M., M.B. JOHNSON, A.M. BONANOS, AND P.E. DIMOTAKIS 2007 Measurements of Molecular Mixing in an Expansion-Ramp Combustor. *21st ICDERS*, Poitiers, France.

BILLIG, F. S., R. BAURLE, AND C. TAM 1999 Design and Analysis of Streamline Traced Hypersonic Inlets. *AIAA Paper* 1999-4974.

BILLIG, F.S., AND A.P. KOTHARI 2000 Streamline Tracing: Techniques for Designing Hypersonic Vehicles, *J. Propulsion and Power*, 16(3):465-471.

BILLIG, F. S., AND L. JACOBSEN 2003 Comparison of Planar and Axisymmetric Flowpaths for Hydrogen Fueled Space AccessVehicles. *AIAA Paper* 2003-4407.

BONANOS, A., J. BERGTHORSON, AND P.E. DIMOTAKIS 2008 Mixing Measurements in a Supersonic Expansion-Ramp Combustor. *Flow, Turbulence and Combustion* 80:489-506.

CANDLER, G.V., T.W. DRAYNA, I. NOMPELIS, M. MACLEAN, M. HOLDEN 2006 HyCAUSE Inward-Turning Inlet Design and CFD Modeling. *JANNAF 29th Airbreathing Propulsion Subcommittee Meeting*, San Diego.

CATRIS, S., AND B. AUPOIX 2000 Density Corrections for Turbulence Models, *Aerospace Science and Technology*, (4):1-11.

CANDLER, G.V., AND T.W. DRAYNA 2008 Design and Optimization of the ASET Inward-Turning Scramjet Inlet. *JANNAF 30th Airbreathing Propulsion Subcommittee Meeting,* Boston.

DIMOTAKIS, P.E. 2005 Turbulent Mixing. *Ann. Rev. Fluid Mech.* 37:329–56.

DRAYNA, T.W., I. NOMPELIS, AND G. V. CANDLER 2006 Hypersonic Inward Turning Inlets: Design and Optimization. *AIAA Paper 2006-0297.*

DUCROS, F., F. LAPORTE, T. SOULÈRES, V. GUINOT, P. MOINAT AND B. CARUELLE 2000 High-Order Fluxes for Conservative Skew-Symmetric like Schemes in Structured Meshes: Application to Compressible flows. *J. Comp. Phys.* 161.

ESTECO, modeFRONTIER, a multi-objective optimization and design environment, AREA Science Park, Padriciano 99, 34012 Trieste, Italy, Version 4.

EVANS, J. S., AND C. J. SCHEXNAYDER 1980 Influence of Chemical Kinetics and Unmixedness of Burning in Supersonic Hydrogen Flames. *AIAA Journal, Vol. 18, No. 2, pp. 188-193.*

FERRANTE, A. AND S.E. ELGHOBASHI 2004 A Robust method for Generating Inflow Conditions for Direct Simulations of Spatially-Developing Turbulent Boundary Layers. *J. Comp. Physics* 198:372-387.

FERRANTE, A., G. MATHEOU, AND P.E. DIMOTAKIS 2010 LES of an Inclined Jet into a Supersonic Turbulent Crossflow: Synthetic Inflow Conditions. *48th AIAA Aerospace Sciences Meeting, AIAA-2009-1511*

FERRANTE, A., C. PANTANO, G. MATHEOU, AND P.E. DIMOTAKIS 2009 On the Effects of the Upstream Conditions on the Transition of an Inclined Jet into a Supersonic Cross-Flow. *47th AIAA Aerospace Sciences Meeting, AIAA-2009-1511.* .

FERRANTE, A., C. PANTANO, G. MATHEOU, AND P.E. DIMOTAKIS, M. STEPHENS, P. ADAMS, R. WALTERS, AND R. HAND 2008 LES of an Inclined Jet into a Supersonic Cross-Flow. *arXiv:0810.1957v1*.

JOHNSON, M.B. 2005 *Aerodynamic Control and Mixing with Ramp Injection*. Engineer's thesis, California Institute of Technology.

KEATING. A., U. PIOMELLI, E. BALARAS. AND H.J. KALTENBACH 2004 *A Priori* and *a Posteriori* tests of Inflow Conditions for Large-Eddy Simulation, *Phys. Fluids*, 16(12).

KOTHARI, A. P., C. TARPLEY, AND T.A. MCLAUGHLIN 1996 Hypersonic Vehicle Design Using Inward Turning Flowfields. *AIAA Paper* 1996-2552.

MADDALENA L., T.L. CAMPIOLI, AND J.A. SCHETZ 2006 Experimental and Computational Investigation of Light-Gas Injectors in Mach 4.0 crossflow. *J. Propulsion and Power, 22:1027–1038.*

MADDALENA, L., S. HOSDER, A. BONANOS, AND P.E. DIMOTAKIS 2008 Extended Conical Flow Theory for Design of Pressure Probes in Supersonic Flows. *47th AIAA Aerospace Sciences Meeting, AIAA-2009-1072*.

MATHEOU, G. 2008 *Large-Eddy Simulation of Turbulent Mixing in a Recirculating Shear Flow*. Ph.D. Thesis California Institute of Technology.

MATHEOU, G., A.M. BONANOS, C. PANTANO, AND P.E. DIMOTAKIS 2010 Large-Eddy Simulation of Turbulent Mixing in a Recirculating Shear Flow. *J. Fluid Mech.* (accepted for publication).

MATHEOU, G., C. PANTANO, AND P.E. DIMOTAKIS 2008 Verification of a Fluid-Dynamics Solver Using Linear Sability Results. *J. Comp. Phys.* 227(11):5385–5396.

MOLDER, S., AND E.J. SZPIRO 1966 Busemann Inlets for Hypersonic Speeds, *Journal of Spacecraft and Rockets,* 3(8):1303-1304.

MUNGAL, M. AND P.E. DIMOTAKIS 1984 Mixing and Combustion With Low Heat Release in a Turbulent Shear Layer. *Physics of Fluids*.12(7):1629-1645.

NIKITIN, N.V., F. NICOUD, B. WASISTHO, AND K.D. SQUIRES 2000 An approach to wall modeling in large-eddy simulations. *J. Fluid Mech*. 148:349–382

NOMPELIS, I., T.W. DRAYNA, AND G.V. CANDLER 2005 A Parallel Unstructured Implicit Solver for Hypersonic Reacting Flow Simulation. *AIAA Paper* 2005-4867.

PANTANO, C., R. DEITERDING, D.J. HILL AND D.I. PULLIN 2007 A Low Numerical Dissipation Patch-Based Adaptive Mesh Refinement Method for Large-Eddy Simulation of Compressible Flows. *J. Comp. Phys.* 221(1):63–87.

PETERSON, D.M., AND G.V. CANDLER 2009 Hybrid RANS/LES of Normal Injection into a Supersonic Crossflow. Submitted to *AIAA J.*

PETERSON D. M., AND G. V. CANDLER 2008 Hybrid RANS/LES of a Supersonic Combustor. *AIAA Paper 2008-6923.*

PROGRAM DEVELOPMENT COMPANY, *GridPro, 300 Hamilton Avenue, Suite 409, White Plains, NY 10601, USA.*

SANTIAGO, J.G., AND J.C DUTTON. 1997 Velocity Measurements of a Jet Injected into a Supersonic Crossflow, *J. Propulsion and Power*, 13(2).

SUBBAREDDY, P., D. PETERSON, G.V. CANDLER, AND I. MARUSIC 2006 A Synthetic Inflow Generation Method Using the Attached Eddy Hypothesis. *AIAA Paper No. 2006-3672*.

SUBBAREDDY, P.K., AND G.V. CANDLER 2009 A Fully Discrete, Kinetic Energy Consistent Finite-Volume Scheme For Compressible Flow, *J. Comp. Phys*., doi:10.1016/j.jcp.2008.10.026.

TEDDER, S. A., S. O. O'BYRNE, P. M. DANEHEY, AND A. D. CUTLER 2005 CARS Temperature and Species Concentration Measurements in a Supersonic Combustor with Normal Injection. *AIAA Paper 2005-0616*.

VAN WIE, D. M., AND S. MOLDER 1992 Application of Busemann Inlet Designs for Flight at Hypersonic Speeds. *AIAA Paper* 1992-1210.

Personnel

Bonanos, Aristides: Postdoctoral Scholar in Aeronautics, Caltech.

Campioli Theresa: Graduate Research Assistant, Aerospace and Ocean Engineering, Virginia Tech.

Candler, Graham (Co-PI): Professor of Aerospace Engineering and Mechanics, University of Minnesota.

Billig, Frederick: Adjunct Professor, Virginia Tech.

Dahl, Earl: Member of the Technical Staff, Aeronautics, Caltech (part-time consultant).

Dimotakis, Paul (PI): John K. Northrop Professor of Aeronautics and Professor of Applied Physics, Caltech, and Chief Technologist, JPL.

Drayna, Travis: Graduate Research Assistant, Aerospace Engineering, University of Minnesota.

Ferrante, Antonino: Postdoctoral Scholar in Aeronautics, Caltech.

Forkel, Elwood: Designer, Aerothermal/Aero-Optical Evaluation Center (AAEC), Buffalo.

Fosbury, Adam: Aeronautical and mechanical engineering undergraduate, State University of New York at Buffalo.

Harvey, John: Consultant, University at Buffalo.

Holden, Michael (Co-PI): Vice-President Hypersonics, Program Manager, Aerothermal Aero-Optical Evaluation Center (AACE), and Adjunct Professor, University at Buffalo.

Jacobsen, Lance (Co-PI): Pyrodyne and Department of Aerospace and Ocean Engineering, Virginia Tech.

Krause, Joseph: aeronautical and mechanical engineering undergraduate, State University of New York at Buffalo.

Lang, Daniel: Research Engineer, Aeronautics, Caltech.

MacLean, Matthew: Senior Scientist, Computational Analysis, State University of New York at Buffalo.

Maddalena, Luca: Postdoctoral Scholar in Aeronautics, Caltech.

Matheou, George: Graduate Research Assistant, and Postdoctoral Scholar in Aeronautics, Caltech.

Meiron, Daniel (Co-PI): Fletcher Jones Professor of Applied and Computational Mathematics and Computer Science, Caltech.

Mojahedi, Christina: Administrative Assistant, Aeronautics, Caltech.

Mundy, Eric: Aeronautical Engineer, Graduate Student, State University of New York at Buffalo.

Nompelis, Ioannis: Postdoctoral Research Associate, Aerospace Engineering, University of Minnesota.

Parker, Ronald: Project manager, aero-optics, LENS/CUBRC

Peterson, David: Graduate Research Assistant, Aerospace Engineering, University of Minnesota.

Rolling, A.J.: Graduate Research Assistant, Aerospace and Ocean Engineering, Virginia Tech

Russo, Salvatore: Instrumentation, Aerothermal/Aero-Optical Evaluation Center (AAEC), Buffalo.

Schetz, Joseph (Co-PI): Fred D. Durham Chair, Department of Aerospace and Ocean Engineering, Virginia Tech.

Smith, Vincent: PE, Mechanical Engineer, Aerothermal/Aero-Optical Evaluation Center (AAEC), Buffalo.

Smolinski, Gregory: Senior Research Engineer, State University of New York at Buffalo.

Subbareddy, Pramod: Graduate Research Assistant, Aerospace Engineering, University of Minnesota.

Throckmorton, Ryan: Graduate Research Assistant, Aerospace and Ocean Engineering, Virginia Tech.

Valiferdowsi, Bahram: Member of Technical Staff, Aeronautics, Caltech.

Wadhams, Timothy: Aeronautical Engineer, Graduate Student, State University of New York at Buffalo.

Wakeman, Thomas: assistant to Ron Parker.

Support for all personnel listed above is part time.

Other collaborators:

Deiterding, Ralph: Senior Postdoctoral Scholar in Applied and Computational Mathematics, Center for Advanced Computing Research, Caltech.

Goodwin, David: Professor Mechanical Engineering and Appl. Physics, Caltech. Author of the *Cantera* software package and collaborator on DNS of hydrocarbon flames.

Hill, David: Postdoctoral Scholar, Aeronautics, Caltech.

Pantano, Carlos: Assistant Professor, Mechanical Engineering, U. Illinois, Urbana-Champagne.

Pullin, Dale: Theodore von Kármán Professor of Aeronautics, Caltech.

Publications of work supported under this grant

Bergthorson, J.M., M.B. Johnson, A.M. Bonanos, M.D. Slessor, W. Su, and P.E. Dimotakis 2008 Molecular mixing and flowfield measurements in a recirculating shear flow. Part I: subsonic flow. *Flow, Turbulence and Combustion* 83(2):153-303.

Bonanos, A., J. Bergthorson, and P.E. Dimotakis 2008 Mixing measurements in a supersonic expansion-ramp combustor. *Flow, Turbulence and Combustion* 80:489-506, doi:10.1007/s10494-008-9133-7.

Bonanos, A.M., J.M. Bergthorson, and P.E. Dimotakis 2008 Molecular mixing and flowfield measurements in a recirculating shear flow. Part II: supersonic flow. *Flow, Turbulence and Combustion* 83(2):251-268.

Ferrante, A., C. Pantano, G. Matheou, and P.E. Dimotakis, M. Stephens, P. Adams, R. Walters, and R. Hand 2008 LES of an inclined jet into a supersonic cross-flow. *arXiv:0810.1957v1*.

Grossman, P., L. Maddalena, and J. Schetz 2007 Wall injectors for high Mach number scramjets. *J. Propulsion and Power* 24(2):259-266.

Maddalena, L., T. Campioli, and J. Schetz 2006 Experimental and computational investigation of light gas injectors in Mach 4.0 cross flow. *J. Propulsion and Power* 22(5):1027-38.

Matheou, G. 2008 Large-eddy simulation of molecular mixing in a recirculating shear flow. *Ph.D. thesis, California Institute of Technology*.

Matheou, G., A.M. Bonanos, C. Pantano, and P.E. Dimotakis 2010 Large-Eddy Simulation of Turbulent Mixing in a Recirculating Shear Flow. *J. Fluid Mech.* (accepted for publication).

Matheou, G., C. Pantano, P.E. Dimotakis 2008 Verification of a fluid-dynamics solver using correlations with linear stability results. *J. Comp. Physics* 227:5385-5396.

Pantano, C., D.I. Pullin, P.E. Dimotakis, and G. Matheou 2008 LES approach for high Reynolds number wall-bounded flows with application to turbulent channel flow. *J. Comp.* 227(21):9271–9291.

Schetz, J.A., L. Maddalena, R. Throckmorton, and R. Neel.2008 Complex wall injector array for high-speed combustors. *J. Propulsion and Power* 24(4):673-680.

Schetz, J.A., 2005 Skin friction measurements in complex turbulent flows using direct methods. 421-430 in engineering turbulence modelling and experiments 6, W. Rodi, Elsevier Ltd., 2005.

Subbareddy P. and G.V. Candler 2008 A fully-discrete, kinetic energy consistent finite-volume scheme for compressible flows. *Journal of Comp. Physics* 228:1347-1364.

Under review and preparation

Peterson, D.M. and G.V. Candler 2009 Hybrid RANS/LES of normal injection into a supersonic crossflow. *AIAA Journal* (submitted).

Conference papers supported under this grant

Bergthorson, J.M., A.M. Bonanos, M.B. Johnson, and P.E. Dimotakis 2008 Measurements of molecular mixing in high-speed flows using fast chemistry. *Proc. 2008 Spring Technical Meeting of the Combustion Institute/Canadian Section*.

Bergthorson, J.M., M.B. Johnson, A.M. Bonanos, and P.E. Dimotakis 2007 Measurements of molecular mixing in an expansion-ramp combustor. *Proc. 21st International Colloquium on the Dynamics of Explosions and Reactive Systems*, Poitiers, France.

Bonanos, A.M., L. Maddalena, and P.E. Dimotakis 2008 Observations on a supersonic shear layer. *47th AIAA Aerospace Sciences Meeting, AIAA-2009-26*.

Bonanos, A., J.M. Bergthorson, and P.E. Dimotakis 2007 Molecular mixing and flowfield measurements in an expansion-ramp combustor: supersonic flow. *43rd AIAA/ASME/SAE/ASEE Joint Propulsion Conference & Exhibit, AIAA-2007-5417*.

Campioli, T., L. Maddalena, and J. Schetz 2006 Studies of shock wave/transverse Injection interaction on supersonic mixing processes. *AIAA-2006-8135*.

Campioli, T., and J. Schetz 2007 Assessment of reacting and nonreacting supersonic mixing," ASME FEDSM2007-37166.

Drayna, T.W., I. Nompelis, and G.V. Candler 2006 Hypersonic inward-turning inlets: Design and optimization. *AIAA-2006-0297.*

Ferrante, A., C. Pantano, G. Matheou, and P.E. Dimotakis 2009 On the effects of the upstream conditions on the transition of an inclined jet into a supersonic cross-flow. *47th AIAA Aerospace Sciences Meeting AIAA-2009-1511*.

Holden, M. S. 2004 Code validation and aerothermal studies of hypersonic vehicle performance in the LENS shock tunnels and expansion tunnel. Invited talk, *5th European Symposium on Aerothermodynamics for Space Vehicles*, Cologne, Germany.

Holden, M.S., T.P. Wadhams, and M. MacLean 2005 Experimental studies to examine viscous interaction and flow chemistry effects of hypersonic vehicle performance. *AIAA 2005-4694, 38th AIAA Thermophysics Conference*, Toronto, Ontario, Canada.

Holden, M.S., T.P. Wadhams, and M. MacLean 2005 Ground tests of full-scale army and DARPA scramjet engines at duplicated flight conditions in the LENS I facility. *JANNAF Meeting*, Charleston, SC.

Holden, M.S. 2005 Aerothermal and propulsion ground testing that can be conducted to increase chances for successful hypervelocity flight experiments. The von Karman Institute. Brussels, Belgium. *Published in RTO course, "Flight Experiments for Hypersonic Vehicle Development."*

Holden, M. S., T.P. Wadhams, G.J. Smolinski, M. MacLean, J. Harvey, and B.J Walker 2006 Experimental and numerical studies on hypersonic vehicle performance in the LENS shock and expansion tunnels. *AIAA 2006-0125, 44th AIAA Aerospace Sciences Exhibit & Meeting*, Reno, NV.

Holden, M.S., G.J. Smolinski, E. Mundy, M. MacLean, T.P. Wadhams, B.J. Walker 2008 Experimental studies for hypersonic vehicle design and code validation of the unsteady flow characteristics associated with "Free Flight" shroud and stage separation and mode switching. AIAA 2008-0642, *46th AIAA Aerospace Sciences Meeting & Exhibit, Reno, NV*.

Holden, M.S., T.P. Wadhams, M. MacLean 2008 Experimental studies in the LENS supersonic and hypersonic tunnels for hypervelocity vehicle performance and code validation. *AIAA 2008-2505*, Dayton, OH.

Holden, M. S., G.J. Smolinski, E. Mundy, M. MacLean, and T.P. Wadhams 2008 full-scale tests of inlet starting, mode switching and component separation at fully duplicated flight conditions. JANNAF 1022, *30th JANNAF Meeting*, Boston, MA.

Maddalena, L., S. Hosder, A. Bonanos, and P. Dimotakis 2008 Extended conical flow theory for design of pressure probes in supersonic flows. *47th AIAA Aerospace Sciences Meeting, AIAA-2009-1072.*

Maddalena, L., J.A. Schetz, and T. Campioli-Shafer 2008 Studies of the detailed vortical structures in a jet in a supersonic crossflow. *AIAA-2008-0087*.

Maddalena, L., J.A Schetz, and R. Neel 2008 Vortex interactions with a jet in a supersonic crossflow. *AIAA-2008-0762*.

Parker, R. A., T. Wakeman, M. MacLean, and M. Holden 2006 Nitric oxide concentration measurements with a quantum cascade laser in the LENS I hypersonic shock tunnel facility. *AIAA 2006-926*, *44th AIAA Aerospace Meeting & Exhibit*, Reno, NV.

Parker, R.A., T.R. Wakeman, M. MacLean, and M. Holden 2006 Nonintrusive measurements of hypersonic engine flowfield using infrared and laser diode diagnostics. *JANNAF Meeting, HyCAUSE Session*, San Diego, CA.

Parker, R., T. Wakeman, M. MacLean, and M. Holden 2007 Measuring nitric oxide freestream velocity using quantum cascade lasers at CUBRC. *AIAA 2007-1329*, *45th Aerospace Meeting & Exhibit*, Reno, NV.

Peterson, D.M. P.K. Subbareddy, and G.V. Candler 2006 DES investigations of transverse injection into supersonic crossflow using a hybrid unstructured solver. *AIAA-2006-0903.*

Peterson, D.M., P.K. Subbareddy, and G.V. Candler 2006 Simulations of injection into a supersonic crossflow using DES with synthetic inflow. *AIAA-2006-3326.*

Peterson, D.M., P.K. Subbareddy, and G.V. Candler 2006 Detached eddy simulations of flush wall injection into a supersonic freestream. *AIAA-2006-4576.*

Peterson, D.M., P.K. Subbareddy, and G.V. Candler 2006 Assessment of synthetic inflow generation for simulating injection into a supersonic crossflow. *AIAA-2006-8128.*

Peterson, D.M., G.V. Candler, and T.W. Drayna 2009 Detached eddy simulation of a generic scramjet inlet and combustor. *AIAA-2009-0130.*

Peterson, D.M., and G.V. Candler 2008 Hybrid RANS/LES of a supersonic combustor. *AIAA-2008-6923.*

Rolling, A.J., and J. Schetz 2006 Direct skin friction measurements with shock-impingement compensation in complex turbulent flows. *AIAA 2006-3838*.

Sang, A., A.J. Rolling, and J. Schetz 2006 A novel skin friction sensor for hypersonic flow. *AIAA 2006-3837*.

Subbareddy, P.K., D.M. Peterson, and G.V. Candler 2006 A synthetic inflow generation method using the attached eddy hypothesis. *AIAA-2006-3672.*

Interactions/Transitions

P.E. Dimotakis discussed scramjet design and mixing with Dr. Campbell Carter of AFRL.

G.V. Candler contributed to the DARPA HyCAUSE program by working directly with Dr. M. Holden of CUBRC on the inward-turning inlet design for the vehicle.

J.A. Schetz presented a Seminar, "Propulsion for Very High-Speed Aircraft" at the Univ. of Michigan in March 2005.

J.A. Schetz served as a Consultant to Dr. Billy Walker of the U.S. Army in Huntsville, AL through a contract with COLSA, Inc. in Huntsville, AL.

J.A. Schetz contributed to the DARPA HyCAUSE program by working directly with Dr. M. Holden of CUBRC on the injector system for the vehicle. Dr. J.A. Schetz also contributed to the scramjet work of Aerojet, Inc. by advising Dr. P.K. Wu on jet injection analysis.

J.A. Schetz has served as a Consultant to Luna Innovations, Inc., Nanosonics, Inc., Aerosoft, Inc. and CraftTech, Inc. on AF, DOD and NASA projects.

Virginia Tech studies on fuel injection and mixing in scramjets have produced results that are being directly applied to AF and DARPA scramjet work.

G.V. Candler's US3D CFD code was transitioned to AFRL/VAAC; POC: Dr. Jonathan Poggie.

New discoveries, inventions, or patent disclosures

Maddalena L., A. M. Bonanos, P. E. Dimotakis and A. Ferrante 2008 A High-spatial-resolution probe, with a simplified calibration technique for simultaneous total and static pressure measurements in supersonic flow with moderate flow angularity and swirl. US Provisional Application No. 29,373 (Filed in 2008)

Honors/Awards

In reverse chronological order:

Honor/Award: Fellow Year received: 2008
Honor/Award Recipient(s): Dimotakis, Paul E.
Awarding Organization: AAAS

Honor/Award: Fellow Year received: 2008
Honor/Award Recipient(s): Candler, Graham V.
Awarding Organization: AIAA

Honor/Award: Thermophysics Award Year received: 2007
Honor/Award Recipient(s): Candler, Graham V.

Awarding Organization: AIAA

Honor/Award: Distinguished McKnight University Professor Year received: 2004
Honor/Award Recipient(s): Candler, Graham V.
Awarding Organization: University of Minnesota

Honor/Award: Leland Atwood Outstanding Aerospace Educator Award Year received: 2004
Honor/Award Recipient(s): Schetz, Joseph A.
Awarding Organization: ASEE/AIAA

Honor/Award: Fellow Year received: 2002
Honor/Award Recipient(s): Holden, Michael S.
Awarding Organization: American Institute of Aeronautics & Astronautics

Honor/Award: Membership Year received: 1998
Honor/Award Recipient(s): Billig, Frederick S.
Awarding Organization: National Academy of Engineering

Honor/Award: Associate Fellow Year received: 1989
Honor/Award Recipient(s): Dimotakis, Paul E.
Awarding Organization: American Institute of Aeronautics & Astronautics

Honor/Award: Fellow Year received: 1985
Honor/Award Recipient(s): Schetz, Joseph A.
Awarding Organization: American Institute of Aeronautics & Astronautics

Honor/Award: Fellow Year received: 1982
Honor/Award Recipient(s): Billig, Frederick S.
Awarding Organization: American Institute of Aeronautics & Astronautics

Honor/Award: Fellow Year received: 1980
Honor/Award Recipient(s): Dimotakis, Paul E.
Awarding Organization: American Physical Society

Honor/Award: Life Fellow Year received: 1980
Honor/Award Recipient(s): Schetz, Joseph A.
Awarding Organization: American Society of Mechanical Engineers

Student theses or dissertations supported under this grant

Author: **Matheou, Georgios**

Affiliation: California Institute of Technology

Type of document: Dissertation

Title: *Large-eddy simulation of molecular mixing in a recirculating shear flow*

The flow field and mixing in an expansion ramp geometry is studied using large-eddy simulation (LES) with subgrid scale (SGS) modeling based on the stretched-vortex model. The expansion ramp geometry was developed to provide enhanced mixing and flameholding characteristics while maintaining low total-pressure losses, elements that are important in the design and

performance of combustors for hypersonic air-breathing propulsion applications. The mixing was studied by tracking a passive scalar without taking into account the effects of chemical reactions and heat release.

In order to verify the solver and the boundary closure implementation, a method utilizing results from linear stability analysis (LSA) theory is developed. LSA can be used to compute unstable perturbations to a flow, subject to certain approximations. First, perturbations are computed using Linear Stability Analysis (LSA). Then these perturbations are used as an inflow condition by the solver being verified. A projection based metric is constructed that only assumes the shape of the solution and not the growth rate of the perturbations, thus also allowing the latter to be determined as part of the verification. The growth rate of the perturbations for an unbounded (effectively) incompressible shear layer and a confined compressible shear layer is found to be in agreement with the prediction of the LSA.

The flow and mixing predictions of the LES are in good agreement with experimental measurements. Total (resolved and subgrid) probability density functions (PDFs) of the passive scalar are estimated using an assumed beta distribution model for the subgrid scalar field. The improved mixing characteristics of the expansion ramp geometry compared to free shear layers are illustrated by the shapes of the PDF;. moreover, the temperature rise and the probability of mixed fluid profiles are in good agreement with the experimental measurements, indicating that the mixing on a molecular scale is predicted correctly by the LES–SGS model. Finally, the predictions of the LES are shown to be resolution-independent. The mean fields and passive scalar PDFs essentially have converged at the two finer grid-resolutions used.

Author: **Johnson, Michael Bernard**

Affiliation: California Institute of Technology

Type of document: Engineer's Thesis

Title: *Aerodynamic control and mixing with ramp injection*

Experiments have been conducted in the GALCIT Supersonic Shear Layer Facility (S3L) to investigate the behavior of a flow and geometry with many features that are potentially useful for a supersonic combustion ramjet (scramjet) engine - a recirculation zone for flameholding, enhanced mixing between fuel and air, and low total-pressure losses. In a subsonic diffuser configuration with no mass injection, the exit velocity and guidewall static pressure profiles collapse over a large range of inlet Reynolds numbers. Significant control of exit velocity and guidewall pressure profiles is possible via injection through a perforated ramp into the freestream. The control authority on the overall pressure coefficient increases with increasing inlet Reynolds number. Simple control volume models put bounds on the overall pressure coefficient for the device.

In low-supersonic flow the area ratio calculated from measured pressures agrees well with the visual shear-layer thickness, illustrating the low total-pressure losses present.

Further control is possible through variable heat release from a fast-chemical reaction between reactants carried in the two streams. At the highest heat release studied, mass injection requirements are lowered by, roughly, a factor of two. Measurements of mixing inferred from the

temperature rise from such a reaction indicate a high level of mixing vs. classical free shear layers. As in free shear layers, however, the level of mixing decreases with increasing heat release.

Author: **Maddalena, Luca**

Affiliation: Virginia Tech

Type of document: Dissertation

Title: *Investigations of injectors for scramjet engines*

An experimental study of an aerodynamic ramp (aeroramp) injector was conducted at Virginia Tech. The aeroramp consisted of an array of two rows with two columns of flush-wall holes that induce vorticity and enhance mixing. For comparison, a single-hole circular injector with the same area angled downstream at 30 degrees also was examined. Test conditions involved sonic injection of helium heated to 313 K to simulate hydrogen into a Mach 4 air cross-stream with average Reynolds number 5.77×10^7 per meter at a jet to freestream momentum flux ratio of 2.1 safely. Sampling probe measurements were utilized to determine the local helium concentration. Pitot and cone-static pressure probes and a diffuser thermocouple probe were employed to document the flow. The main results of this work were that the mixing efficiency value of this aeroramp design that was optimized at Mach 2.4 for hydrocarbon fuel, which was only slightly higher than that of the single-hole injector at these flow conditions and the mass-averaged total pressure loss parameter showed that the aero-ramp and single-hole injectors had the same overall losses.

The natural extension of the investigation was then to look in detail at two major physical phenomena that occur in a complex injector design, such the Aeroramp: the jet-shock interaction and the interaction of the vortical structures produced by the jets injection into a supersonic cross flow. Experimental studies were performed to investigate the effects of impinging shocks on injection of heated helium into a Mach 4 crossflow. It was found that the addition of a shock behind gaseous injection into a Mach 4 crossflow enhances mixing only if the shock is closer to the injection point, where the counter-rotating vortex pair (always associated with transverse injection in a crossflow) is not formed yet, and the deposition of baroclinic generated of vorticity is the highest.

The final investigation concerned the interaction of the usual vortex structure produced by jet injection into a supersonic crossflow and an additional axial vortex typical of those that might be produced by the inlet of a scramjet or the forebody of a vehicle to be controlled by jet interaction phenomena. The additional axial vortices were generated by a strut-mounted, diamond cross-section wing mounted upstream of the injection location. The wing was designed to produce a tip vortex of strength comparable to that of a typical counter-rotating vortex pair (CVP) found in the plume of a jet in a crossflow. The profound interaction of supersonic vortices supported by a quantitative description and characterization of the flowfield has been demonstrated.

Author: **Rolling, August**

Affiliation: Virginia Tech

Type of document: Dissertation

Title: *Design of gages for direct skin friction measurements in complex turbulent flows with shock impingement compensation*

This research produced a new class of skin friction gages that measures wall shear even in shock environments. One test specimen separately measured wall shear and variable-pressure induced moment. Through the investigation of available computational modeling methods, techniques for accurately predicting gage physical responses were developed. The culmination of these model combinations was a design optimization procedure. This procedure was applied to three disparate test conditions: 1) short-duration, high-enthalpy testing, 2) blow-down testing, and 3) flight testing. The resulting optimized gage designs were tested virtually against each set of nominal load conditions. The finalized designs each successfully met their respective test condition constraints while maximizing strain output due to wall shear.

These gages limit sources of apparent strain: inertia, temperature gradient, and uniform pressure. A unique use of bellows provided a protective shroud for surface strain gages. Oil fill provided thermal and dynamic damping while eliminating uniform pressure as a source of output voltage. Two Wheatstone bridge configurations were developed to minimize temperature effects, first from temperature gradient and then from spatially varying heat flux induced gradient. An inertia limiting technique was developed that parametrically investigated mass and center-of-gravity impact on strain output.

Multiple disciplinary computational simulations of thermal, dynamic, shear, moment, inertia, and instrumentation interaction were developed. Examinations of instrumentation error, settling time, filtering, multiple input dynamic response, and strain gage placement to avoid thermal gradients were conducted. Detailed mechanical drawings for several gages were produced for fabrication and future testing

Author: **Campioli, Theresa Lynn**

Affiliation: Virginia Tech

Type of document: Dissertation

Title: *Computational studies of penetration and mixing for complex jet injectors to aid in design of hypersonic systems*

A computational study of sonic light-gas jet injection into a supersonic cross flow was conducted at Virginia Tech. The scope of the numerical analysis encompassed many studies that affect how the flow field is modeled numerically and the behavior, specifically mixing, of the flow field itself. A single, round injector was used for the baseline design. Simulated conditions involved sonic injection of helium heated to 313 K into a Mach 4 air cross stream with average Reynolds number 5.77 $x10^7$ per meter and a freestream momentum flux ratio of 2.1. The primary numerical flow solver used was GASP v. 4.2. The Menter Shear Stress Transport (SST) turbulence model was used, since the algorithm has good capability of solving both wall-bounded and free-shear flows. The SST model was able to capture the mixing behavior of the complex flow-field.

Important numerical parameters that affect the capabilities of the numerical solver were studied for the baseline injector. These sensitivity studies varied the choice of turbulent Prandtl number, Schmidt number, freestream turbulence intensity, boundary layer size, steady and unsteady approaches, and computational software packages. A decrease in the turbulent Prandtl number resulted in better mixing of the prediction and better agreement with the experiment. An increase in the turbulent Schmidt number has a small adverse effect on the predictions. The mixing characteristics remained constant with an increase in freestream turbulence intensity. A decrease in boundary layer height had a significant adverse affect on the mixing behavior of the prediction. The best baseline design then was compared to three different injector configurations: an aerodynamic ramp consisting of four injectors, a diamond injector aligned with the flow and the diamond injector yawed 15º to the oncoming flow. The CFD tools were more accurate in the prediction of the aeroramp injector than the diamond-shaped injectors. The aeroramp injector slightly improved mixing efficiency over the Baseline injector at these conditions. Both of the diamond-shaped injectors had similar mixing as the Baseline injector but did not predict significant improvement in penetration for the analyzed conditions.

Additional studies involving the interaction of transverse injection with impinging oblique shock waves were performed. The CFD predicted larger improvements than the experimental results with the shock impinging further from the jet. The impingement of a shock upon light gas jet injection increased mixing. The closer the shock is to the injection point, the larger the effect on mixing and vorticity. The last analyses involved a numerical comparison of a non-reacting, frozen flow model to a reacting hydrogen-air model. The reacting analysis prediction had an improved spreading rate and larger CVP with downstream distance over the non-reacting analysis. The mixing was not altered by the addition of hydrogen/air reactions to the numerical equations. The numerical tools used are capable of predicting the complex flow field of jet injection into a supersonic freestream with proper choice of models and parameters. Numerical modeling offers a way to study the entire flow field thoroughly in a cost-and time-efficient manner.

Author: **Subbareddy, Pramod Kumar**

Affiliation: University of Minnesota

Type of document: Dissertation

Title: *Stable low-dissipation schemes for turbulent compressible flows*

Shock capturing schemes, which are commonly used in compressible flow simulations, introduce excessive amounts of numerical viscosity that smear out small scale flow features. A few low-dissipation methods have been proposed in the recent literature. They are more selective in the sense that they explicitly identify the portion of the numerical flux that is diffusive and damp its effect in 'smooth' regions of the flow. This work employs flux vector splitting methods. The dissipative portions of the Steger-Warming schemes are identified explicitly, and various shock detection switches are explored.

For high Reynolds number flows, especially when the energetic scales are close to the Nyquist limits of the grids used, aliasing errors become noticeable. These high frequency oscillations, which arise due to the nonlinear nature of the Navier-Stokes equations cause solutions to become unstable. When dissipative methods are used, these errors are suppressed; however, when using low-dissipation schemes, they can be prominent and need to be addressed by some other means.

In this thesis we focus on methods that enhance stability by enforcing 'secondary conservation' -- the fluxes are constrained in such a way that a conservation law for a secondary, positive quantity also is satisfied. In particular, we focus on kinetic energy, and a fully discrete (in time and space) 'kinetic energy consistent' scheme is derived and tested.

Hybrid RANS-LES methods such as detached eddy simulations (DES) are necessary in order to make simulations of high speed flows with attached boundary layers affordable. A popular DES model is based on the Spalart-Allmaras (S-A) RANS equation. A minor modification to the length scale makes the model behave in a hybrid manner. The S-A model itself was constructed using mostly empirical arguments by the authors. This model is analyzed, and its connection to other turbulence models, in particular the subgrid-scales kinetic energy (ksgs) equation, is explored. A dynamic version of the model is proposed and tested on simulations of decaying isotropic turbulence.